

Review

Not peer-reviewed version

---

# Gadolinium Nanoparticles: Emerging Platforms Beyond Imaging for Drug Delivery and Theranostics

---

[Amir Nasrolahi Shirazi](#)<sup>\*</sup>, [Rajesh Vadlapatla](#), [Ajay Koomer](#), Heyam Zayed, Paris Marabut, [Keykavous Parang](#)

Posted Date: 25 February 2026

doi: 10.20944/preprints202602.1422.v1

Keywords: gadolinium nanoparticles; drug delivery; metal nanoparticles



Preprints.org is a free multidisciplinary platform providing preprint service that is dedicated to making early versions of research outputs permanently available and citable. Preprints posted at Preprints.org appear in Web of Science, Crossref, Google Scholar, Scilit, Europe PMC.

Copyright: This open access article is published under a [Creative Commons CC BY 4.0 license](#), which permit the free download, distribution, and reuse, provided that the author and preprint are cited in any reuse.

Disclaimer/Publisher's Note: The statements, opinions, and data contained in all publications are solely those of the individual author(s) and contributor(s) and not of MDPI and/or the editor(s). MDPI and/or the editor(s) disclaim responsibility for any injury to people or property resulting from any ideas, methods, instructions, or products referred to in the content.

Review

# Gadolinium Nanoparticles: Emerging Platforms Beyond Imaging for Drug Delivery and Theranostics

Amir Nasrolahi Shirazi <sup>1,\*</sup>, Rajesh Vadlapatla <sup>1</sup>, Ajoy Koomer <sup>1</sup>, Heyam Zayed <sup>1</sup>, Paris Marabut <sup>1</sup> and Keykavous Parang <sup>2</sup>

<sup>1</sup> Department of Pharmaceutical Sciences, College of Pharmacy, Marshall B. Ketchum University, 2575 Yorba Linda Blvd., Fullerton, CA 92831, USA

<sup>2</sup> Center for Targeted Drug Delivery, Department of Biomedical and Pharmaceutical Sciences, Chapman University School of Pharmacy, Harry and Diane Rinker Health Science Campus, 9401 Jeronimo Rd, Irvine, CA 92618, USA

\* Correspondence: ashirazi@ketchum.edu

## Abstract

Gadolinium nanoparticles (GdNPs) have gained increasing attention as multifunctional metal-based nanoplatforms that extend far beyond their traditional use as magnetic resonance imaging (MRI) contrast agents. Their specific magnetic properties, tunable physicochemical features, and tunable biocompatibilities with biocompatible coatings give them great potential as drug delivery and theranostic applications. They offer better stability, less systemic toxicity, and more surface modification options compared to molecular gadolinium chelates. Thermal decomposition, hydrothermal synthesis, polyol-based processes, and green methodologies, along with functionalization products that employ polymers, peptides, or targeting ligands, have significantly enhanced colloidal stability as well as biodistribution and selective accumulation at disease sites. Functionalized GdNPs exhibit outstanding properties not only as drug carriers for their specific indications but also as agents for multiple imaging modalities with superior therapeutic efficacy through radiosensitization and magnetically assisted delivery. Conjugation with ligands consisting of RGD peptides, hyaluronic acid, or folic acid allows receptor-mediated targeting and enhances the uptake into cellular tissue in tumors. It is also important to mention that GdNP-based formulations have been proved to exert synergistic effects when administered in combination with chemotherapeutic agents like doxorubicin, paclitaxel, and cisplatin. Although GdNPs have shown interesting preclinical findings, clinical translation of the products is limited due to scale-up limitations, long-term safety challenges, pharmacokinetics, and regulatory problems. This review presents synthetic strategies for the use of GdNPs, their main physicochemical and magnetic properties, ligand engineering for targeted delivery, and underlying biological mechanisms of their theranostic performance.

**Keywords:** gadolinium nanoparticles; drug delivery; metal nanoparticles

## 1. Introduction

### 1.1. Inorganic Nanoparticles in Drug Delivery

Inorganic nanoparticles containing metals can be divided into three major categories, including metal nanoparticles, metal oxide nanoparticles, and quantum dots.

**Metal nanoparticles** (MNPs) are nanomaterials composed of a single elemental metal and can exist as individual atoms or clusters of many atoms [1,2] Common examples include Au, Ag, Pt, Cu, Pd, Re, Zn, Ru, Co, Cd, Al, Ni, and Fe [3–5], and most metals can be synthesized into nanoparticles using either top-down or bottom-up approaches [6]. They are typically produced as colloidal suspensions or solid particles through straightforward fabrication methods such as bio-assisted

synthesis, hydrothermal processing, and microwave-assisted techniques. These nanoparticles exhibit distinctive physicochemical properties including size, surface-to-volume ratio, pore size, electronic surface charge, structural characteristics (crystalline or amorphous), morphology (spherical or cylindrical), and sensitivity to external factors (e.g., humidity, temperature, light) along with exceptional functional features such as localized surface plasmon resonance (LSPR), high chemical reactivity, and broad electromagnetic absorption. Their enhanced optical, optoelectronic, catalytic, and antimicrobial/anticancer/antiviral activities further contribute to their broad utility across diverse applications [7,8].

**Metal oxide nanoparticles** are produced by altering the properties of their parent metals. For example, iron-based nanoparticles (FeNPs) readily oxidize to iron oxide at room temperature in the presence of oxygen, resulting in increased reactivity compared with unoxidized FeNPs [9,10]. Most metal oxide NPs are synthesized through physical or chemical methods, as these materials can be reduced in size by mechanical forces (e.g., within a rotating reactor) or through their heightened chemical reactivity [11]. Commonly fabricated examples include aluminum oxide ( $\text{Al}_2\text{O}_3$ ), iron oxide ( $\text{Fe}_2\text{O}_3$ ), magnetite ( $\text{Fe}_3\text{O}_4$ ), silicon dioxide ( $\text{SiO}_2$ ), and titanium dioxide ( $\text{TiO}_2$ ). These nanoparticles generally exhibit enhanced properties such as improved surface area, catalytic activity, tunable electronic, optimal properties, and biological interactions relative to the bulk metals from which they are derived [3,12].

**Quantum dots** are nanoscale semiconductor particles distinguished by their extremely small size and unique optical characteristics. Typically composed of materials such as cadmium selenide (CdSe), cadmium telluride (CdTe), or lead sulfide (PbS), they generally range from 2 to 10 nm in diameter. Owing to their tunable emission properties and high photostability, quantum dots are employed in a wide range of applications, including display technologies, solar cells, and bioimaging [13].

This review focuses on MNPs, with particular emphasis on gadolinium nanoparticles (GdNPs) as emerging multifunctional nanoplatforms in biomedical applications. First, we provide a concise overview of the use of metal nanoparticles in drug delivery and compare major classes of systems, including AuNP, iron oxide, and GdNPs, with respect to their physicochemical properties, imaging capabilities, biocompatibility, and therapeutic potential.

## 1.2. Metal Nanoparticles in Drug Delivery

MNPs have attracted significant interest in nanomaterials research because of their distinctive size-dependent properties and broad functional versatility. Their tunable size, high surface reactivity, and capacity to integrate multiple functions such as simultaneous targeting and imaging, along with the ability to support controlled drug release, provide MNPs with notable advantages over many other drug-delivery platforms [1].

Widely studied MNPs include gold (AuNPs), silver (AgNPs), iron oxide ( $\text{Fe}_3\text{O}_4$  NPs), platinum (Pt NPs), zinc oxide (ZnO NPs), selenium (SeNPs), and GdNPs. These nanomaterials can be produced by chemical, physical, or biological synthesis methods and have been widely studied because of their remarkable properties, enabling their use for various therapeutic, medical, and diagnostic purposes [14].

$\text{Fe}_3\text{O}_4$  NPs possess superparamagnetic properties, which allow them to be directed by external magnetic fields and to work as competent magnetic resonance imaging (MRI) contrast agents. When functionalized with polymers or peptides, these nanoparticles can be guided with high accuracy to tumors or inflamed tissues, thereby enhancing targeted drug delivery [15]. Additionally, their inherent biocompatibility and biodegradability support their integration into advanced theranostic platforms, where they enhance cellular internalization and controlled release of therapeutics such as 5-fluorouracil (5-FU) [16].

ZnO NPs display potent pH-sensitive properties that allow them to disintegrate selectively in the acidic environment of tumor tissues. These controlled break-downs facilitate localized release of the drug and are also responsible for the generation of reactive oxygen species (ROS), which further

strengthen cytotoxic effects against cancer cells. Collectively, these properties characterize ZnO NPs as potential candidates for targeted cancer therapy. Together, these properties position ZnO NPs as compelling candidates for targeted cancer therapy [17].

MNPs have many properties and particular applications, but selenium nanoparticles (SeNPs) have shown particularly promising activity as they possess anti-oxidant, anticancer, and immunomodulatory properties [18]. They inhibit tumor progression by inducing apoptosis and regulating redox homeostasis yet exhibit minimal toxicity toward normal cells [19]. Functionalization with targeting molecules or therapeutic compounds further improves their precision and efficacy, making SeNPs attractive platforms for delivering chemotherapeutics and natural bioactives in the treatment of cancer, cardiovascular disorders, and inflammatory diseases [20].

Gd-based materials have been extensively used in biomedical applications, particularly as contrast agents in MRI, owing to the strong paramagnetic properties of  $Gd^{3+}$  ions [21,22]. GdNPs, traditionally used as MRI contrast agents owing to Gd's pronounced paramagnetism, are now being advanced into sophisticated theranostic systems. Embedding imaging functionality into other modalities (e.g., targeted drug delivery, photothermal therapy) facilitates real-time visualization of disease sites and enables treatment. This combined diagnostic–therapeutic capability provides significant advantages in cancer management; accurate monitoring and localized intervention are essential aspects of this approach [23]. Based on the functionalized MNPs, we discussed and reported on AuNPs, SeNPs, and GdNPs, emphasizing their multifunctional capabilities and significant potential to improve drug delivery applications [24–28]. We further reviewed recent progress in selenium nanoparticle–based drug delivery [29].

In this review, we present a comprehensive and integrated analysis of Gd's physiological and biochemical roles, together with an in-depth examination of GdNPs. We describe the complete repertoire of synthesis strategies, including chemical, physical, and biologically inspired approaches, as well as key physicochemical parameters, such as particle size, morphology, surface charge, and colloidal stability. Moreover, we present current strategies for ligand design and surface functionalization to facilitate drug delivery and improve therapeutic performance. In advancing on the previous research question, we further identify the biological targets for which GdNPs are engineered, elucidate the mechanisms underlying their therapeutic actions, and discuss the key challenges and limitations still hindering their development and clinical translation. Lastly, we discuss emerging trends and future directions that are likely to shape the evolution of GdNP-based nanomedicine.

### 1.3. Gadolinium (Gd)

Gd, a group IIIB lanthanide, is among the most abundant rare earth elements (REEs) found in the Earth's crust [30]. The chemical behavior of most lanthanides is fairly similar, which explains why, in all, it took more than a century to split them into individual elements. The magnetic properties of Gd, in particular, are unique and explain many of its applications [31]. Element 64 is located halfway through the lanthanide 4f series, and the trivalent  $Gd^{3+}$  ion can organize its seven 4f electrons in a half-filled shell with all spins parallel, a magic member, which represents the maximum possible number within the lanthanide series. Although europium also possesses seven 4f electrons in its neutral state,  $Eu^{3+}$  lacks unpaired electrons and consequently does not exhibit comparable magnetic behavior. The unusually high number of unpaired electrons gives Gd (III) the largest possible total spin  $S=7/2$ , and a correspondingly very large spin magnetic moment. This characteristic can be used to improve the performance of permanent magnets. The 4f shell of lanthanides has electron binding energies in the valence range, making it possible to chemically vary the 4f occupation, but the compact 4f radial size is typical of the outermost core electrons and prevents most 4f electrons from directly participating in bond formation [32].

However, because the orbital angular momentum of  $Gd^{3+}$  is effectively zero, its total magnetic moment arises almost entirely from electron spin. As a result, the experimentally observed and

theoretically predicted magnetic moments of  $Gd^{3+}$  (approximately 7.90 and 7.94, respectively) place it below several other lanthanides in overall magnetic strength, despite its high spin contribution [33].

Unlike most other REEs, Gd exhibits exceptionally strong paramagnetic behavior [34], a property that underpins its widespread use as a “contrast agent” in MRI. When Gd accumulates in tissues, it significantly shortens  $T_1$  relaxation times, resulting in enhanced signal intensity (brightness) on  $T_1$ -weighted MRI scans [35]. The MRI signal comes from certain nuclear spins, such as the ubiquitous protons. That nuclear spin system, however, is heated by the radiofrequency field used for magnetic resonance. This heating typically weakens the MRI signal [21]. The large electronic magnetic moment of Gd (III) helps couple the nuclear spin systems to the “lattice” and keep it cool. This is called nuclear spin-lattice relaxation. To avoid health hazards, because  $Gd^{3+}$  is somewhat toxic, the Gd ion is surrounded by chelating ligands that prevent it from entering tissues [36]. New ligands are under development to improve safety [37].

Glycosaminoglycans (GAGs) are the primary contributors to the fixed charge density (FCD) of cartilage and are among the first components to be depleted during the early stages of arthritic disease. Beshir et al. hypothesized that, similar to sodium ions ( $Na^+$ ), the negatively charged contrast agent  $Gd-DTPA^{2-}$ —and the resulting changes in proton  $T_1$  relaxation—could be used to quantify tissue FCD and thereby estimate GAG concentration. For example, when complexed with the chelating agent, diethylenetriamine penta-acetic acid (DTPA),  $Gd-DTPA^{2-}$  affects the  $T_1$  MRI signal. Because of its charge,  $Gd-DTPA^{2-}$  has been used to measure the fixed charge density (FCD) for cartilage, which correlated with FCD measurements of explanted cartilage made using other techniques [38] as well as with the dynamic modulus and the sulfated glycosaminoglycan (GAG) content of bioreactor cultured cartilage [39]. Further,  $Gd-DTPA^{2-}$  has been used to measure the FCD of engineered cartilage constructs consisting of chondrocytes cultured in a poly(ethylene oxide) diacrylate hydrogel [40,41]. In another application,  $Gd-DTPA^{2-}$  has been used to label albumin to allow quantification of protein concentration profiles using MRI [42]. In contrast to  $Gd-DTPA^{2-}$ , iron oxide serves as a superparamagnetic MRI contrast agent, which shortens  $T_2$  relaxation times.  $Fe_3O_4$  NPs have been used to label stem cells for in vivo MRI detection [43].

Beyond diagnostic imaging, the unique magnetic properties of Gd-based materials enable the generation of localized magnetic microenvironments. These microenvironments can be exploited to fabricate non-contact biological scaffolds, thereby supporting tissue engineering, 3D cell culture, and regenerative medicine applications [44–46].

Gd-containing compounds also contribute to bone-related processes by suppressing osteoclast activity, stimulating the differentiation of stem cells into osteoblasts, and promoting vascular development, all of which support osteogenesis [47,48]. Comparable to other REEs, Gd can enhance the antimicrobial activity of carrier materials by modulating their surface charge and improving their photothermal behavior [49].

In oncology, Gd-based platforms offer multiple therapeutic and diagnostic capabilities. They serve as effective contrast agents for tumor visualization and as nanocarriers for targeted drug delivery. Once localized at the tumor site, these materials can disrupt mitochondrial integrity, interfere with ATP production, and trigger oxidative stress, collectively driving tumor cell death and enabling multimodal anticancer action.[50–52] Gadolinium oxide ( $Gd_2O_3$ ) in particular has demonstrated broad utility, including applications in drug delivery, cancer cell targeting and imaging, therapeutic intervention, cell labeling and tracking, and biosensing [53].

In addition to its biological applications, gadolinium (Gd) plays a significant role in magnetic cooling technologies. In this process, known as the magnetocaloric effect, magnetic material increases in temperature when exposed to an external magnetic field due to the alignment of its magnetic dipoles. Conversely, when the magnetic field is removed under adiabatic (thermally isolated) conditions, the material undergoes cooling. By modulating the applied magnetic field and controlling thermal insulation, entropy is exchanged between the electronic spin system and the lattice degrees of freedom, enabling refrigeration [54].

#### 1.4. Gadolinium Nanoparticles (GdNPs)

GdNPs have emerged as a versatile class of nanomaterials with significant potential in biomedical imaging and theranostic applications. These nanoparticles containing Gd with seven unpaired 4f electrons exhibit strong paramagnetic properties, making them particularly effective as MRI contrast agents. These properties impact water molecules' T1 and T2 relaxation times [55,56]. When engineered at the nanoscale, Gd-based materials can overcome several limitations associated with conventional low-molecular-weight Gd chelates, including rapid renal clearance, limited tissue retention, and concerns related to Gd deposition [57,58].

GdNPs can be synthesized using a range of chemical, physical, and biological approaches, yielding diverse nanostructures such as gadolinium chloride [59], gadolinium oxide (Gd<sub>2</sub>O<sub>3</sub>) [60], gadolinium fluoride (GdF<sub>3</sub>) [61], and hybrid or core-shell nanoparticles [62]. Their physicochemical characteristics, particle size, morphology, crystallinity, and surface charge critically influence magnetic relaxivity, colloidal stability, biodistribution, and cellular uptake [53,63]. In many cases, nanoscale Gd formulation demonstrates enhanced longitudinal (T1) relaxivity compared with molecular chelates, attributed to increased rotational correlation times and higher local Gd density [64].

Surface functionalization plays a pivotal role in improving the biocompatibility and multifunctionality of GdNPs. Coatings based on polymers, silica, peptides, lipids, or biomolecules are frequently employed to stabilize nanoparticles, reduce Gd ion leakage, and enable active targeting toward specific biological markers [65–67]. Through rational ligand design, GdNPs have been developed as multifunctional platforms capable of MRI contrast enhancement, targeted drug delivery, photothermal therapy, and radiosensitization, supporting their application in theranostic systems [68–70].

Despite their promising performance, the clinical translation of GdNPs requires careful consideration of their safety and long-term fate.

The issue of Gd release, bioaccumulation, and systemic toxicity, particularly in patients with renal insufficiency, may be a concern [71,72]. Therefore, existing researchers are working in the exploration of novel nanoparticle formulations, biodegradable coatings, and comprehensive in vivo assessments to get better pharmacokinetic as well as clearance properties [53,73]. By and large, GdNPs are a robust and versatile nanotechnology platform for novel diagnostic and therapeutic strategies. Advanced synthesis methodology, surface engineering, and biological assessment progress is anticipated to be important for extending their precision medicine and targeted drug delivery functions [74].

## 2. Chemistry of GdNPs

This chemical versatility enables GdNPs to function as safe, traceable, and highly adaptable nanocarriers, bridging diagnostic imaging with targeted and controlled therapeutic delivery. The drug delivery chemistry of GdNPs relies on precise control of inorganic core composition, surface functionalization, and stimulus-responsive conjugation strategies.

From a drug delivery perspective, the chemistry of GdNPs is carefully designed to integrate high magnetic performance with efficient cargo loading, targeting, and controlled release. Gd is typically incorporated as Gd<sup>3+</sup> within chemically stable inorganic matrices such as gadolinium oxide, fluoride, or hybrid organosilicate frameworks, which act as nanocarriers while minimizing the dissociation of free Gd<sup>3+</sup> ions during systemic circulation [72–74]. These solid matrices provide structural robustness, protect encapsulated therapeutics, and enable simultaneous imaging and therapy, positioning GdNPs as ideal theranostic platforms.

**Synthesis.** GdNPs are not formed spontaneously from elemental Gd but are synthesized through controlled chemical processes that convert gadolinium ions (Gd<sup>3+</sup>) into nanoscale solid materials. Typically, a soluble gadolinium salt such as gadolinium chloride or nitrate is dissolved in aqueous or organic media, where it dissociates into Gd<sup>3+</sup> ions. These ions are then reacted with

precipitating agents (e.g., hydroxide, fluoride, or phosphate sources) under carefully controlled pH, temperature, and concentration. When supersaturation is reached, nucleation occurs, forming small crystalline clusters that grow into nanoparticles such as  $\text{Gd}_2\text{O}_3$ ,  $\text{GdF}_3$ , or  $\text{GdPO}_4$ . Careful control of nucleation and growth is essential because particle size, crystallinity, and morphology strongly influence magnetic relaxivity and biomedical performance [75].

**Stabilization.** To preserve nanoscale dimensions and prevent aggregation, stabilizing agents such as polymers [76], surfactants [77], peptides [25], or silica coatings are introduced during or after synthesis. Common fabrication strategies include co-precipitation, hydrothermal/solvothermal synthesis, and thermal decomposition, each offering distinct advantages in size uniformity and structural control [78]. In many biomedical applications, Gd is incorporated into or doped within stable nanomatrices (e.g., silica or iron oxide) to minimize the release of free  $\text{Gd}^{3+}$  ions, which may pose toxicity concerns. Subsequent surface functionalization enables improved biocompatibility, targeting capability, and drug-loading efficiency, thereby transforming Gd from a simple paramagnetic ion into a multifunctional theranostic nanoplatform [75].

**Coordination.** GdNPs, like other members of the lanthanide family, function as a hard Lewis acid and therefore favor predominantly ionic interactions with coordinating species [79]. All GdNP chelates currently used in clinical and therapeutic applications are derived from octadentate polyaminocarboxylate ligand frameworks (**Figure 1**).

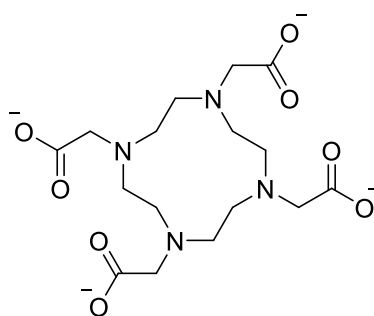


**Figure 1.** Chemical structure of octadentate polyaminocarboxylate.

These ligands coordinate strongly to the  $\text{Gd}^{3+}$  ion, occupying eight of its nine preferred coordination sites. The remaining coordination position is typically filled by a water molecule, which plays a key role in modulating proton relaxation in magnetic resonance imaging. Chelation involves the formation of stable five-membered rings through coordination of nitrogen and carboxylate donor atoms to the metal center. These chelate rings are generated through metal–ligand ionic interactions and differ fundamentally from classical five-membered organic heterocycles, such as furan, which are stabilized by covalent bonding rather than metal coordination [79].

The coordination chemistry and size control of GdNPs also influence intracellular trafficking, drug release, and clearance. Ultrasmall and biodegradable GdNP formulations have been shown to facilitate renal clearance following drug delivery, reducing long-term tissue retention and toxicity risks [72,80]. Importantly, the strong  $T_1$  relaxivity of Gd enables real-time MRI tracking of nanoparticle biodistribution and drug delivery efficiency, providing direct feedback on therapeutic localization and treatment response [64,72–74].

**Surface chemistry.** The surface chemistry of GdNPs is central to drug loading and delivery efficiency. Therapeutic agents, including chemotherapeutic drugs, radiosensitizers, nucleic acids, and photosensitizers, can be physically encapsulated within porous structures or chemically conjugated to surface functional groups via covalent or electrostatic interactions [72,81,82]. Carboxylate-, phosphonate-, and silane-based chemistries are commonly employed to anchor drugs either directly or through stimulus-responsive linkers. These linkers can be engineered to respond to acidic pH, redox gradients, or enzymatic activity, enabling site-specific drug release in tumor microenvironments or intracellular compartments [73,83].

Chemical functionalization further enables multimodal and targeted drug delivery. Polymeric coatings, particularly polyethylene glycol (PEG), are frequently grafted onto GdNP surfaces to enhance colloidal stability, prolong circulation time, and reduce nonspecific protein adsorption [71,72,74]. Targeting ligands, such as peptides, antibodies, or small molecules, can be conjugated via orthogonal surface reactions, promoting receptor-mediated uptake and increasing drug accumulation at diseased sites [74,84–86]. This modular surface chemistry allows independent optimization of pharmacokinetics, targeting specificity, and therapeutic payload.

### 3. Absorption, Distribution, and Elimination of GdNPs

GdNPs have recently gained importance as an alternative to low-molecular-weight Gd chelates by means of increased relaxivity, increased imaging sensitivity, and potential for multifunctional theranostic use [75,87,88]. In contrast to molecular Gd complexes, GdNPs display unique pharmacokinetic profiles determined by their nanoscale dimensions, surface chemistry, and structural organization. Given this, knowledge of these pharmacokinetic profiles should be complemented to optimize imaging performance whilst minimizing toxicity and long-term tissue retention.

The selected studies summarized in this section demonstrate that the pharmacokinetics of Gd-based agents, whether formulated as conventional chelates or nanoscale constructs, are governed by a complex interplay of molecular stability, physicochemical properties, and biological handling.

The pharmacokinetic behavior of Gd is defined by its absorption, distribution, metabolism, and excretion (ADME), which differ markedly from those of small-molecule Gd agents [89,90]. Following intravenous administration, GdNPs rapidly interact with plasma proteins and elements of the mononuclear phagocyte system, influencing circulation half-life and biodistribution [91].

Physicochemical parameters such as particle size, shape, surface charge, and surface functionalization, including polymeric, peptide-based, or ligand-directed coatings play critical roles in determining organ accumulation, particularly in the liver, spleen, kidneys, and tumor tissues [92–94]. Strategic surface engineering has been shown to modulate pharmacokinetics by prolonging systemic circulation, enhancing renal clearance, or promoting active targeting of diseased tissues [95,96].

Excretion pathways are a central consideration in the pharmacokinetics of GdNPs, especially in light of increasing concerns regarding Gd retention and associated toxicities [57,97,98]. Ultrasmall GdNPs with hydrodynamic diameters below the renal filtration threshold may undergo efficient renal clearance, whereas larger or aggregated systems are more likely to be eliminated through hepatobiliary routes, increasing the risk of long-term tissue accumulation [84,99].

Furthermore, the thermodynamic and kinetic stability of Gd within the nanoparticle matrix is a key determinant of biosafety, as dissociation and release of free Gd<sup>3+</sup> ions have been linked to adverse outcomes such as nephrogenic systemic fibrosis and persistent tissue deposition [100–102]. Consequently, rigorous pharmacokinetic evaluation remains essential for the safe and effective translation of GdNPs into clinical imaging and theranostic applications.

Neburkova et al. [103] reported that gadolinium can accumulate in the brain after GBCA administration. They demonstrated that trace amounts of Gd<sup>3+</sup> released from GBCAs form Gd<sup>3+</sup>-ferritin nanoparticles at nanomolar concentrations under physiological conditions. Structural analysis showed that Gd<sup>3+</sup> binds to the surface of the ferritin oxyhydroxide core, and this process is driven by the kinetic instability of the GBCA rather than its thermodynamic stability. The formation of these Gd<sup>3+</sup>-ferritin complexes in serum may partly explain the increased T1 signal intensity observed in ferritin-rich brain regions after repeated GBCA exposure.

Gd deposition in patients with normal renal function was first described by Kanda et al. [Kanda 2014], who observed T1-weighted hyperintensity in the globus pallidus and dentate nucleus following multiple doses of linear GBCAs. Later studies confirmed that these signal changes are associated with Gd retention and raised concerns about potential long-term neurotoxicity

[98,104,105]. Although macrocyclic GBCAs appear to result in lower brain accumulation than linear agents, they are not entirely free from deposition [106–111].

The kidney is also recognized as a primary site of Gd retention in both humans and animal models. Differences in renal persistence among macrocyclic agents have been reported, but it remains uncertain whether MRI can accurately detect residual renal Gd or determine whether it is retained as intact GBCA or transformed chemical species.

Mounting evidence indicates that repeated exposure to Gd-based contrast agents (GBCAs) leads to Gd deposition in the brain and peripheral organs long after administration, yet the biodistribution and chemical form of retained Gd remain poorly understood. Le Fur et al. (2023) compared the pharmacokinetics, distribution, and speciation of four GBCAs, gadoterate, gadoteridol, gadobutrol, and gadobenate in healthy rats using MRI, mass spectrometry, elemental imaging, and electron paramagnetic resonance spectroscopy, alongside analysis of human kidney specimens [112]. They performed their *in vivo* investigation using 32 rats that received a dose of Gadoteric acid, gadoteridol, gadobutrol, or Gadobenate (2.0 mmol/kg) for 10 consecutive days. The structures of these compounds are illustrated in **Figure 2**.

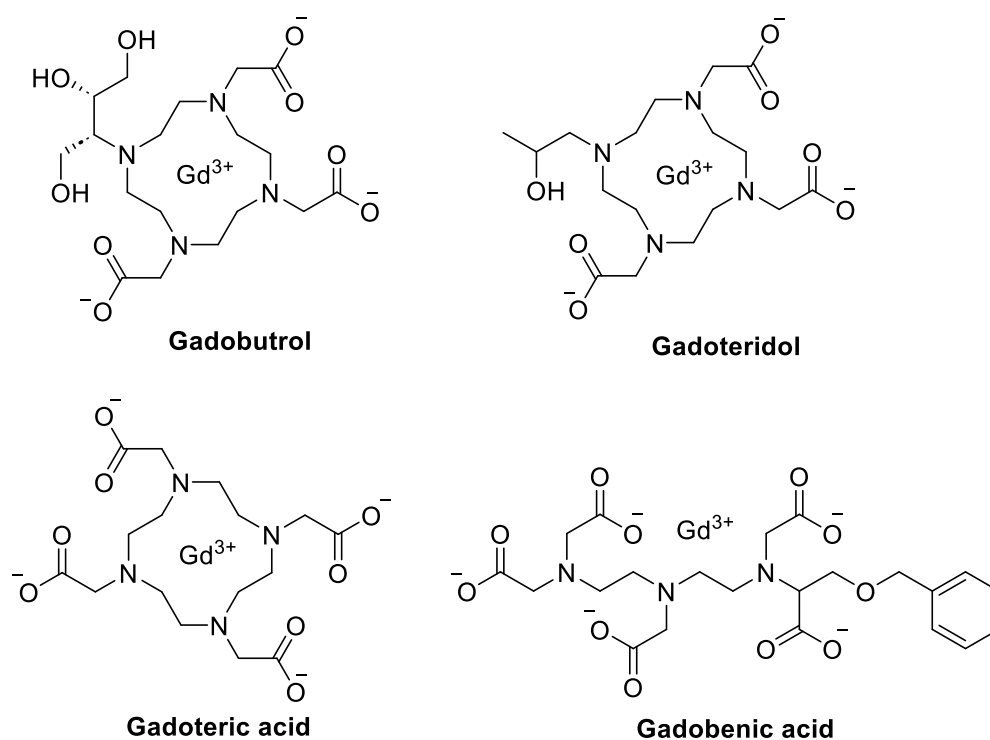


**Figure 2.** The chemical structures of gadoteric acid, gadoteridol, gadobutrol, and gadobenate.

GBCA-naïve rats served as controls in a longitudinal study in which three-dimensional T1-weighted UTE MRI and R2\* maps of the kidneys were acquired at 3, 17, 34, and 52 days post-injection, and gadolinium levels in 23 organs, tissues, and fluids were quantified by mass spectrometry at 17 and 52 days, with renal distribution and cortical speciation further characterized by elemental imaging and EPR spectroscopy; statistical analyses included ANOVA, Kruskal–Wallis, response profile analysis, and Pearson correlation, and Gd concentrations in multiple organs, including the kidney cortex and medulla, were reported in nmol/g wet tissue [112]. Analysis of human kidney samples revealed detectable Gd weeks after GBCA exposure, with higher levels in patients receiving multiple doses, supporting prolonged renal retention; among the agents evaluated, gadoteridol showed the most efficient elimination, followed by gadoterate, gadobutrol, and gadobenate, and although the kidneys exhibited the highest Gd concentrations overall, significantly lower renal cortex retention was observed for gadoteridol compared with gadobutrol and gadobenate at 52 days post-

injection, with no evidence of renal injury. R2\* mapping proved more sensitive than T1-weighted MRI for detecting renal Gd and correlated strongly with ex vivo Gd concentrations, whereas T1-weighted imaging failed to detect high retained levels, and EPR spectroscopy confirmed that Gd was primarily retained as intact chelates [112]. In a separate investigation, Guenther et al. (2025) evaluated the pharmacokinetics of gadoquatrane (**Figure 3**), a tetrameric, macrocyclic, extracellular Gd-based MRI contrast agent with high relaxivity and kinetic stability currently in Phase 3 clinical development, in female cynomolgus monkeys and compared it with established macrocyclic agents using analytically distinguishable lanthanide analogs; following intravenous administration, gadoquatrane demonstrated a rapid, multiphasic plasma decline characterized by fast distribution, efficient systemic elimination, and a slow terminal phase, yielding an effective half-life of approximately 1 hour, along with a low volume of distribution and clearance values consistent with extracellular, renally eliminated contrast agents [113].

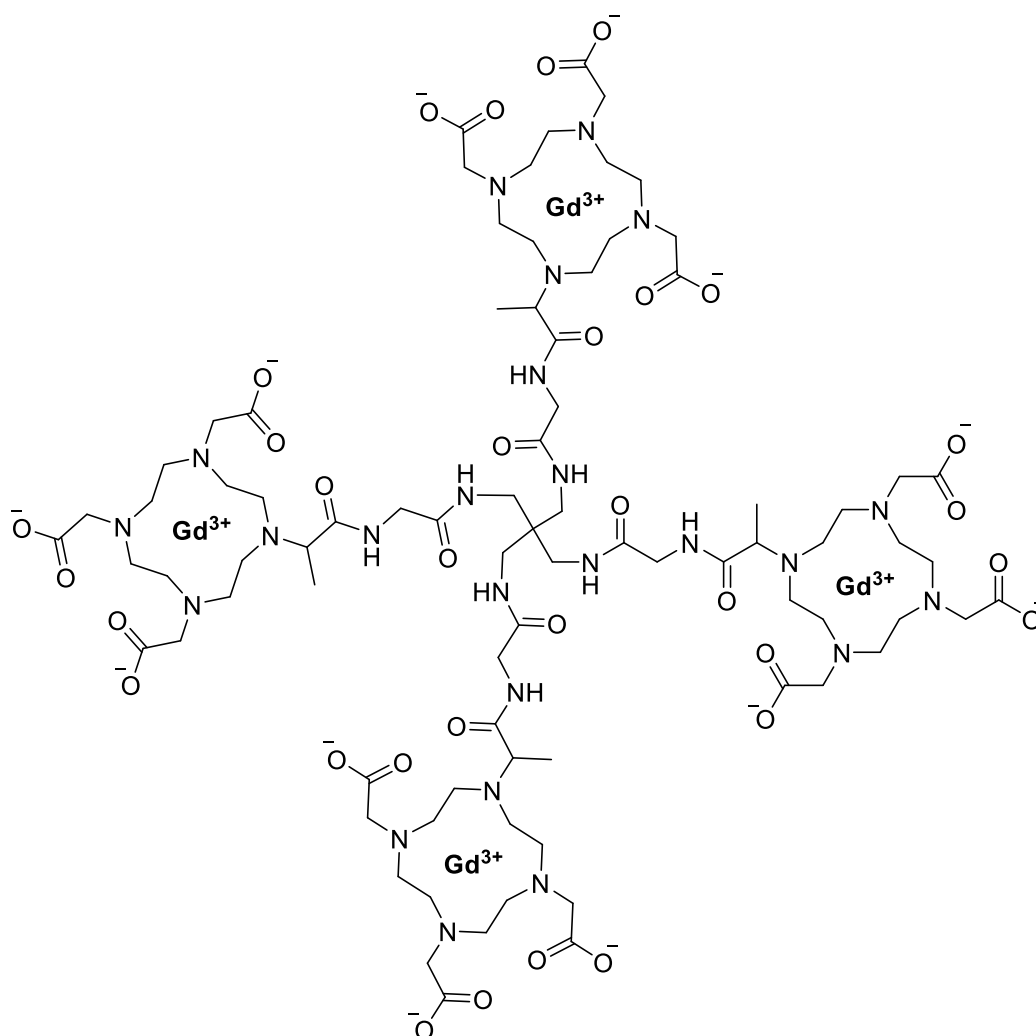


**Figure 3.** The chemical structures of tetrameric gadoquatrane.

Gadoquatrane was rapidly and almost exclusively excreted via the kidneys, with approximately 97% of the administered dose recovered in urine within 24 h. Residual urinary excretion persisted at very low levels over extended periods, while tissue retention was minimal and decreased substantially over time, with the highest concentrations observed in the kidney cortex and markedly lower levels in skin and brain. Tissue concentrations declined between early and late sampling time points, and no metabolic degradation products were detected, confirming the compound's metabolic stability. The pharmacokinetic behavior and tissue distribution of gadoquatrane in nonhuman

primates were comparable to those of established macrocyclic contrast agents, with no evidence of increased long-term Gd retention [113].

Moreover, the excretion of gadopentetate dimeglumine (**Figure 4**) into human breast milk was evaluated in 20 lactating women following intravenous administration of a standard clinical dose [114]. Serial milk samples collected over 24 h demonstrated that Gd transfer into breast milk was minimal, with a cumulative excretion of less than 0.04% of the administered dose in all subjects. The mean excreted fraction was approximately 0.009%, corresponding to absolute amounts in the micromolar range. Based on these findings, the estimated oral exposure of a nursing infant would be more than two orders of magnitude lower than the approved intravenous dose for neonates, indicating negligible clinical risk. These results suggest that routine interruption of breastfeeding for 24 h after gadopentetate dimeglumine administration may not be necessary.

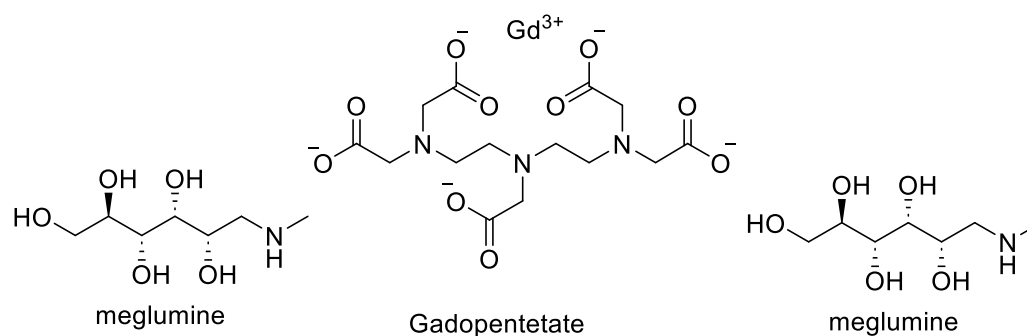


**Figure 4.** The chemical structures of gadopentetate dimeglumine.

Furthermore, Hahn et al. (2009) reported a clinical study with a focus on pharmacokinetics and safety of gadobutrol, (**Figure 2**) an extracellular Gd-based MR contrast agent in pediatric patients aged 2–17 years undergoing routine contrast-enhanced MRI or MR angiography [115]. Across age groups, gadobutrol pharmacokinetics were well described by a two-compartment model with renal elimination from the central compartment. Body weight–normalized clearance and volume of distribution values were consistent with those observed in adults and showed predictable variation with body weight, while age itself did not independently influence pharmacokinetic parameters. Following administration, plasma Gd concentrations simulated fell within expected ranges across the pediatric weight spectrum, supporting comparable systemic exposure between children and adults when dosed on a per-kilogram basis. Most doses of gadobutrol were eliminated through the kidneys, with approximately 77% of the dose being excreted in the urine within 6 h, confirming rapid renal clearance in pediatric patients. The agent was tolerated well and only a small percentage of patients were affected by mild drug-related adverse reactions. Disparities in gadobutrol pharmacokinetics in children are largely associated with body weight rather than age, and support the use of the standard weight-based adult dose (0.1 mmol/kg) in pediatric patients of 2–17 years old without titrating the dose [115].

In general, macrocyclic GBCAs exhibit favorable kinetic stability and rapid renal elimination, but mounting evidence indicates that measurable amounts of Gd can persist in the brain, kidneys, and other tissues for extended periods, even in individuals with normal renal function. The kidney, in particular, emerges as a key reservoir for residual Gd, with agent-dependent differences in retention and clearance that are not reliably captured by conventional T1-weighted MRI. Additionally, results in the generation of Gd<sup>3+</sup>–ferritin nanoparticles reveal that in vivo the possibility of secondary nanoparticle-like species can arise, which challenges the assumptions about Gd speciation and toxicity. Therefore, rigorous pharmacokinetic and speciation investigations, advanced imaging and analytical methods, and rational material design should be the prerequisite for safe development and clinical translation of the next-generation GdNPs and contrast agents.

## 4. GdNPs in Drug Delivery

GdNPs have emerged as multifunctional platforms in drug delivery to their unique electronic structure and high atomic number. GdNPs serve as valuable nanocarrier design tools, as the incorporation of Gd allows precise control over nanoparticle size, morphology, and surface charge. Particle size critically influences pharmacokinetics, tumor accumulation via the enhanced permeability and retention effect, and intracellular trafficking, while surface charges modulate cellular uptake, endosomal escape, and interactions with serum proteins. Positively charged GdNPs often exhibit enhanced cellular internalization, whereas negatively charged or neutral surfaces can improve colloidal stability and circulation time [92,93,116]. Herein, we summarize different roles of GdNPs in drug delivery systems.

### 4.1. Used as Photo-Thermal Nanoparticles and Work Through Increasing Energy

On one hand, GdNPs can be used in photothermal or energy-amplifying agents where they facilitate local energy generation under external stimuli like near-infrared (NIR) light, X-ray irradiation, or radiofrequency fields. Excited GdNPs can convert the absorbed energy to heat. The localized hyperthermia caused then promotes tumor cell death and the improvement of therapeutic efficacy by increasing membrane permeability and facilitating drug release. GdNPs can also be used as radiosensitizers in radiation-induced energy deposition and ROS generation in tumor tissues.

Another great example is AGuIX<sup>®</sup> nanoparticles [120]. AGuIX<sup>®</sup> nanoparticles (Activation and Guiding of Irradiation by X-ray) are ultrasmall (~3–5 nm) polysiloxane-based GdNPs designed as theranostic agents for MRI-guided radiotherapy. Structurally, they consist of a rigid polysiloxane matrix covalently grafted with gadolinium chelates (typically DOTA-type ligands), enabling high Gd payload per particle while maintaining strong kinetic stability. Their small hydrodynamic diameter permits renal clearance, reducing long-term tissue retention. Functionally, AGuIX<sup>®</sup> nanoparticles act as  $T_1$  MRI contrast agents due to the paramagnetic properties of Gd<sup>3+</sup> and simultaneously serve as radiosensitizers: the high atomic number of Gd enhances local dose deposition during irradiation, increasing ROS generation and amplifying tumor cell damage. These particles preferentially accumulate in tumors via the enhanced permeability and retention (EPR) effect and have progressed into clinical evaluation for image-guided radiotherapy in brain metastases and other solid tumors.

When these compounds are engineered to absorb NIR or radiofrequency energy, Gd-containing nanostructures, including gadolinium oxide nanoparticles, Gd-doped hybrid nanoparticles, and Gd-integrated nanocomposites can generate heat through non-radiative relaxation processes [75,84]. This photothermal effect enables spatially controlled hyperthermia, which can directly induce cancer cell death and simultaneously enhance drug delivery by increasing membrane permeability, promoting endosomal escape, and accelerating drug release from thermoresponsive carriers [121,122]. The high atomic number and paramagnetic properties of Gd further allow seamless integration of photothermal therapy with MRI-guided treatment, enabling real-time monitoring of nanoparticle accumulation and therapeutic response [49].

In drug delivery applications, the photothermal energy generated by GdNPs can be exploited to trigger on-demand drug release and enhance therapeutic efficacy through synergistic mechanisms. Localized heating can disrupt tumor vasculature, improve intratumoral drug penetration, and sensitize cancer cells to chemotherapeutic agents or radiotherapy by increasing intracellular stress and impairing DNA repair pathways [51,52,123–126]. Additionally, Gd-doped photothermal systems have been shown to enhance ROS generation and immune activation when combined with other treatment modalities, further amplifying antitumor effects [128,129]. These energy-mediated functions position Gd-based photothermal nanoparticles as powerful components of advanced drug delivery systems, particularly for image-guided, stimuli-responsive, and combination cancer therapies.

Zhao et al. (2020) developed multifunctional GdPO<sub>4</sub>/CS/Fe<sub>3</sub>O<sub>4</sub> composite scaffolds for simultaneous photothermal tumor ablation and bone regeneration in breast cancer bone metastasis

by hydrothermally synthesizing hydrated  $\text{GdPO}_4 \cdot \text{H}_2\text{O}$  nanorods ( $\approx 80$  nm width, 3  $\mu\text{m}$  length) at 180  $^\circ\text{C}$  for 24 h and integrating them with  $\text{Fe}_3\text{O}_4$  nanoparticles ( $\sim 20$  nm) into a chitosan matrix via freeze-drying, yielding highly porous scaffolds with interconnected macropores ( $\sim 100$   $\mu\text{m}$ ). Under 808 nm near-infrared (NIR) irradiation (4.6  $\text{W}/\text{cm}^2$ ), the  $\text{GdPO}_4/\text{CS}/\text{Fe}_3\text{O}_4$  scaffolds rapidly increased temperature from 20  $^\circ\text{C}$  to 47.7  $^\circ\text{C}$  within 10 min, whereas control scaffolds lacking  $\text{Fe}_3\text{O}_4$  remained below 29  $^\circ\text{C}$ ; in vivo, local temperatures reached  $\sim 45.4$   $^\circ\text{C}$  within 20 s, inducing significant tumor apoptosis and marked tumor diameter reduction after 14 days of treatment. Beyond photothermal efficacy, the scaffolds demonstrated strong osteogenic capacity, with minimal ion release after 120 h of degradation (1.58  $\mu\text{M}$   $\text{Gd}^{3+}$  and 1.37  $\mu\text{M}$  Fe, within safe biological limits). In rat calvarial defect models (5 mm defects), new bone volume/tissue volume (BV/TV) reached  $58.15 \pm 3.45\%$  ( $\text{GdPO}_4/\text{CS}$ ) and  $61.23 \pm 2.12\%$  ( $\text{GdPO}_4/\text{CS}/\text{Fe}_3\text{O}_4$ ), significantly higher than blank control ( $10.01 \pm 1.86\%$ ) and CS alone ( $19.16 \pm 2.87\%$ ), with mineralization rates of  $5.62 \pm 0.38$  and  $6.19 \pm 0.31$   $\mu\text{m}/\text{day}$ , respectively, more than double that of CS ( $2.57 \pm 0.41$   $\mu\text{m}/\text{day}$ ). Mechanistically, controlled  $\text{Gd}^{3+}$  release promoted M2 macrophage polarization and activated the BMP-2/Smad/RUNX2 pathway, enhancing VEGF-mediated angiogenesis and osteogenic differentiation, thereby integrating localized photothermal therapy with accelerated vascularized bone regeneration in a single dual-functional platform for treating breast cancer bone metastases [129].

Cui et al. (2024) integrated MRI contrast capability, microwave-induced immunogenic cell death, and checkpoint blockade to achieve synergistic thermotherapy and immunotherapy with strong tumor inhibition and favorable biosafety. They reported the design of a microwave-responsive Gd metal organic framework (Gd-MOF) nanosystem (Gd/MPC) for MRI-guided thermotherapy combined with PD-1 checkpoint blockade immunotherapy. The nanosystem was fabricated by first synthesizing Gd-MOF (Gd/M), followed by loading with the anti-PD-1 antibody (aPD-1) with a quantified loading proportion of 28.23%. A phase change material (1-tetradecanol, melting point 38–40  $^\circ\text{C}$ ) was incorporated at a mass ratio of approximately 28%, enabling temperature-triggered drug release. Finally, SCC7 cancer cell membranes were coated onto the surface, increasing the hydrodynamic diameter from approximately 163 nm (Gd/MP) to 182 nm (Gd/MPC), consistent with a 5–10 nm membrane layer. Under microwave irradiation (0.6  $\text{W}/\text{cm}^2$ ), a 1 mg/mL Gd/MPC solution exceeded 45  $^\circ\text{C}$  within 5 min., whereas the medium alone only reached  $\sim 40$   $^\circ\text{C}$ . At higher microwave power (up to 1.0  $\text{W}/\text{cm}^2$ ) or concentration (up to 4 mg/mL), heating showed clear power- and concentration-dependence. Importantly, even with 15 mm pork tissue coverage, the temperature still increased efficiently, demonstrating strong tissue penetration. In vitro, microwave-treated Gd/MPC raised local temperatures to near 50  $^\circ\text{C}$ , completely suppressing SCC7 proliferation over 48 h, while Gd/MPC alone (100–200  $\mu\text{g}/\text{mL}$ ) showed minimal cytotoxicity, confirming thermal-specific tumor killing [130].

Under in vivo experiment, C3H mice bearing SCC7 tumors ( $\sim 50$   $\text{mm}^3$  at treatment initiation) were divided into seven groups ( $n = 5$  per group). After intravenous injection, microwave irradiation (0.6  $\text{W}/\text{cm}^2$ , 10 min) was applied 4 h post-injection, coinciding with peak tumor accumulation detected by fluorescence and MRI. Tumor temperatures in the Gd/MPC + MW group approached 55  $^\circ\text{C}$ , compared to  $\sim 50$   $^\circ\text{C}$  with microwave alone. By day 12, the Gd/MPC + MW group showed the strongest tumor suppression, significantly outperforming PBS, Gd/M, and aPD-1 alone groups. Quantitatively, the MOF delivery system improved antitumor efficacy by  $\sim 26\%$  compared to free aPD-1; microwave hyperthermia contributed  $\sim 15\%$  additional inhibition; incorporation of aPD-1 increased efficacy by 59% compared to Gd/M alone; and homologous membrane coating added a further 15% improvement [130].

Jiang et al. (2021) demonstrated a highly effective, low-toxicity MRI-guided photothermal chemotherapy system with strong tumor imaging, controlled drug release, and synergistic antitumor efficacy for TNBC. They developed a multifunctional theranostic nanoplatform based on Gd-encapsulated carbon dots (Gd@CDs) for magnetic resonance imaging (MRI)-guided photothermal chemotherapy of triple-negative breast cancer (TNBC). The Gd@CDs were synthesized via a hydrothermal method using 3,4-dihydroxyhydrocinnamic acid, ethylenediamine, and  $\text{GdCl}_3$  at 200

°C for 5 h. HRTEM analysis showed spherical nanoparticles with an average core diameter of 2.58 nm and a lattice spacing of 0.16 nm, while dynamic light scattering indicated a hydrodynamic size of 308.8 nm due to aggregation. ICP-MS confirmed a Gd content of 0.459%. The carbon dots exhibited excitation-dependent fluorescence with a maximum emission at 437 nm (excitation 360 nm), a fluorescence lifetime of 3.58 ns, and a quantum yield of 26.84%. Importantly, Gd@CDs demonstrated a 6.53-fold higher longitudinal relaxation rate ( $R_1$ ) compared to clinical Gd-DTPA at the same Gd concentration, indicating superior  $T_1$  MRI contrast capability. In vitro cytotoxicity tests showed >90% viability of 293T cells even at 1 mg/mL after 24 h, and in vivo studies in mice (0.3 and 3 mg/kg injections for 16 days) showed no significant changes in liver or kidney biochemical markers, confirming good biocompatibility [131].

The therapeutic platform was constructed by loading doxorubicin (Dox) and the NIR photothermal agent IR825 onto Gd@CDs, forming Dox@IR825@Gd@CDs. Drug loading efficiencies were 16.4% for Dox and 8.9% for IR825, with encapsulation efficiencies of 68.8% and 83.3%, respectively. Under acidic conditions (pH 4.92), 76.4% of Dox was released within 120 h, compared to 55.6% at pH 7.38, indicating tumor-microenvironment-responsive release. Upon 808 nm laser irradiation (3 W, 5 min), a 1 mg/mL solution showed a temperature increase of 25.4 °C to approximately 57 °C, and maintained photothermal stability over five irradiation cycles. In vitro, combined photothermal chemotherapy reduced 4T1 cell viability to about 26% at 0.2 mg/mL under irradiation, and at 0.5 mg/mL more than 97% of cells were killed. In vivo, tumor-bearing mice treated with Dox@IR825@Gd@CDs plus NIR irradiation exhibited the strongest tumor suppression over 14 days, with tumor accumulation reaching 5.4% injected dose per gram (ID/g). No significant body weight loss or motor coordination impairment (rotarod test) was observed [131]. **Table 1** elaborates on gadolinium-based nanoparticles that function with their photothermal properties and their energy modalities.

**Table 1.** Gd-based photothermal nanoparticles across increasing energy modalities.

Nanoparticle/System	Energy Modality	Major Results	Key Drug-Delivery / Theranostic Implications	Reference
Gd <sub>2</sub> O <sub>3</sub> nanoparticles; Gd-doped hybrid nanostructures	Radiofrequency (RF), NIR light	Efficient non-radiative relaxation → localized heat generation	Hyperthermia	[128]
GdPO <sub>4</sub> /CS/Fe <sub>3</sub> O <sub>4</sub> scaffold	808 nm NIR laser	Temp ↑ 20 → 47.7 °C in 10 min; tumor apoptosis; BV/TV bone regeneration ↑ to ~61%	Dual-functional platform for tumor ablation + bone regeneration drug delivery	[129]
Microwave-responsive Gd-MOF (Gd/MPC) + anti-PD-1 antibody	Microwave irradiation	Temp ↑ >45 °C in 5 min; tumor inhibition ↑ ~26% vs free drug	Temperature-triggered immunotherapy drug release	[130]
Gd@Carbon dots loaded with Dox + IR825	808 nm NIR laser	Temp ↑ to ~57 °C; >97% tumor cell kill; strong MRI contrast	Controlled drug release + imaging-guided therapy	[131]

#### 4.2. Surface, Size, and Charge Modification of GdNPs for Drug Delivery

GdNPs enhance drug delivery efficiency by enabling precise regulation of nanoparticle size and surface charge, two fundamental parameters that govern circulation behavior, tumor accumulation, cellular uptake, and intracellular trafficking [132]. The unique coordination chemistry of gadolinium ions (Gd<sup>3+</sup>) enables strong, stable interactions with chelating ligands, peptides, polymers, and inorganic matrices, facilitating the rational design of nanostructures with controlled size distributions and high structural stability [133,134] By acting as a coordination center or crosslinking element, Gd contributes to the formation of compact, uniform nanoparticles, minimizing aggregation and ensuring reproducible drug loading and release characteristics.

The capacity of GdNPs to simultaneously regulate size and surface charge could enable the creation of highly tunable drug delivery platforms with optimized pharmacokinetics, enhanced tumor selectivity, and improved intracellular drug delivery. This physicochemical versatility, combined with Gd's intrinsic imaging and radiosensitizing properties of Gd, positions GdNPs as powerful multifunctional nanocarriers for advanced cancer drug delivery and theranostic applications.

Control of nanoparticle size is particularly critical for optimizing in vivo drug delivery. GdNP-based systems can be engineered within the optimal size window of approximately 10–100 nm, which favors passive tumor targeting via the enhanced permeability and retention (EPR) effect while limiting premature renal clearance and excessive uptake by the mononuclear phagocyte system [132]. Smaller GdNPs exhibit improved tumor penetration and diffusion through dense tumor matrices, whereas moderately larger constructs benefit from prolonged blood circulation and higher drug payload capacity [74,133]. This size tunability allows Gd-based nanocarriers to be tailored for specific therapeutic objectives, including deep tumor penetration, sustained drug release, or combined diagnostic–therapeutic (theranostic) applications.

For example, Siribbal et al. (2024) reported the hydrothermal synthesis of hollow Gd<sub>2</sub>O<sub>3</sub> nanocarriers (~100–120 nm in diameter) using carbon nanospheres (~200 nm) as sacrificial templates, followed by calcination at 800 °C to generate porous hollow structures. The nanocarriers exhibited longitudinal and transverse relaxivities of  $r_1 = 1.8 \text{ s}^{-1}\cdot\text{mM}^{-1}$  and  $r_2 = 5.3 \text{ s}^{-1}\cdot\text{mM}^{-1}$  (1.41 T, 40 °C), confirming their potential as positive MRI contrast agents. To improve biocompatibility and reduce Gd<sup>3+</sup> ion leaching, the particles were coated with citric acid (CA), which significantly enhanced cell viability. While bare Gd<sub>2</sub>O<sub>3</sub> showed toxicity above 5 µg/mL, CA-capped nanocarriers maintained ~100–120% cell viability after 48 h, even at concentrations up to 100 µg/mL [135].

Drug loading and release studies were conducted using Congo red (CR) and sparfloxacin (SP). CA functionalization markedly improved loading capacity, increasing CR loading from 6.75% (bare) to 20% (CA-capped). Under physiological conditions (pH 7.4, 37 °C), bare particles released ~80% of CR within 8 h and nearly all within 24 h, whereas CA-coated carriers provided sustained release up to 96 h. For SP, CA-capped nanocarriers achieved 4% loading (vs. 1.78% for bare nanocarriers) and demonstrated prolonged antibiotic release for up to 168 h, maintaining effective antibacterial activity at concentrations as low as 0.03 mg/mL against both *E. coli* and *S. aureus*. Additionally, confocal microscopy confirmed time-dependent cellular internalization within 10 min to 24 h, highlighting the dual imaging and drug delivery capability of the hollow Gd<sub>2</sub>O<sub>3</sub> platform [135].

Surface charge modulation represents another key mechanism through which GdNPs improve drug delivery performance. GdNPs can be readily functionalized with positively or negatively charged ligands, such as amine-rich polymers, carboxylated coatings, or zwitterionic molecules, enabling fine control over electrostatic interactions with biological environments [136]. Positively charged GdNPs exhibit enhanced cellular internalization due to electrostatic attraction to negatively charged cell membranes and nucleic acids, making them particularly effective for delivering DNA, siRNA, mRNA, and nucleus-targeting chemotherapeutic agents [63,137]. Additionally, cationic surface charge promotes endosomal escape by destabilizing the membrane, further improving intracellular drug bioavailability.

Conversely, negatively charged or near-neutral GdNPs reduce nonspecific protein adsorption and opsonization in the bloodstream, thereby prolonging systemic circulation and improving tumor accumulation [132]. Charge-shielding strategies, such as PEGylation or charge-reversible surface coatings, can be combined with Gd-based cores to achieve stimulus-responsive charge switching neutral during circulation and positively charged within the acidic tumor microenvironment, thereby maximizing both safety and therapeutic efficacy [138 Mi 2020]. Importantly, the ability to finely balance surface charge could also reduce off-target toxicity and minimize immune recognition.

In addition to engineering surface chemistry, particle size, and charge to optimize circulation time and cellular uptake, gadolinium-based nanoparticles (GdNPs) have been extensively functionalized with polymers, inorganic nanostructures, peptides, and therapeutic payloads to

enhance drug loading efficiency, targeting, and controlled release. For example, polymer-coated composites, hollow and mesoporous Gd<sub>2</sub>O<sub>3</sub> structures, cyclic peptide–Gd assemblies, and albumin-coated nanocarriers have demonstrated improved drug encapsulation, pH-responsive or sustained release, enhanced intracellular transport, or synergistic anticancer activity. Table 2 shows selected functionalized GdNP drug-delivery platforms highlighting how polymer, peptide, inorganic, and albumin coatings enhance loading efficiency, targeting, and therapeutic outcomes.

**Table 2.** Representative functionalized GDNPs for enhanced drug delivery, targeting, and controlled release.

GdNP System / Functionalization	Therapeutic Payload	Key Structural Features	Drug Delivery / Biological Outcome	Reference
Chitosan-coated ZnO/TiO <sub>2</sub> /Gd <sub>2</sub> O <sub>3</sub> nano-composite (RNC)	Rapamycin	Crystalline ZnO, TiO <sub>2</sub> , Gd <sub>2</sub> O <sub>3</sub> ; chitosan coating	100% drug loading; sustained release; ROS amplification; apoptosis; G0/G1 arrest in A549 cells	[139]
Solid vs hollow Gd <sub>2</sub> O <sub>3</sub> nanospheres with ZnO coating	Doxorubicin	Hollow spheres (~120 nm) with high BET surface area	pH-responsive release; theranostic imaging capability	[140]
Cyclic peptide-GdNPs [(WR) <sub>5</sub> C-Gd]	Small-molecule drugs; siRNA	Star-shaped nanoparticles (240–260 nm); cationic peptide surface	6-fold increased intracellular delivery; enhanced platinum drug efficacy; >10-fold siRNA uptake and STAT-3 knockdown	[25]
Gd-doped hollow CeO <sub>2</sub> –ZrO <sub>2</sub> nanoplatform (PEGylated)	Doxorubicin	Mesoporous hollow structure; high surface area; PEG coating	pH-responsive release; dual MRI/CT imaging; strong tumor growth inhibition in vivo	[141]
Albumin-coated Gd <sub>2</sub> O <sub>3</sub> nanoparticles (Gd <sub>2</sub> O <sub>3</sub> @BSA)	Curcumin	Core <10 nm; hydrodynamic size 17–26 nm; stable colloidal surface	pH-responsive release; high biocompatibility; enhanced cytotoxicity toward nasal carcinoma cells	[142]

Ganesh et al. (2025) developed a rapamycin-loaded, chitosan-coated ZnO/TiO<sub>2</sub>/Gd<sub>2</sub>O<sub>3</sub> nanocomposite (RNC) to enhance drug bioavailability and overcome multidrug resistance in non-small cell lung cancer (NSCLC) using A549 cells, with structural characterization confirming crystalline ZnO (wurtzite), Gd<sub>2</sub>O<sub>3</sub> (cubic), and TiO<sub>2</sub> (anatase) phases, and FTIR and EDX analyses verifying successful chitosan coating and rapamycin incorporation. Drug-loading studies showed that 150 mg of the composite achieved 100% loading efficiency for 400 µg rapamycin, corresponding to 3.75 µg composite per 1 µg drug, substantially exceeding previously reported lipid–polymer systems (~67.8%); in vitro release experiments demonstrated complete diffusion of free rapamycin within 3 h, whereas the RNC enabled sustained and controlled release with 100% drug release over 6 h, indicating improved delivery and potential bioavailability [139 Ganesh 2025]. Biologically, the RNC exhibited enhanced anticancer efficacy, with an LC<sub>50</sub> of 31 µg/mL against A549 cells compared to 32 µg/mL for free rapamycin, while maintaining lower toxicity toward normal L929 cells (103 µg/mL for RNC vs. 100 µg/mL for rapamycin), demonstrating selective cytotoxicity; reactive oxygen species (ROS) levels increased markedly from 1,221 AU (control) to 4,592 AU (rapamycin) and further to 10,281 AU with RNC treatment, nearly threefold higher than the free drug. Flow cytometry revealed a reduction in viable cells from 95% (control) to 46.9% following RNC treatment, accompanied by increased early apoptosis (10.6%) and total cell death (19.4%), as well as pronounced G0/G1 cell cycle arrest (80.5%) compared with 65.9% for rapamycin alone, alongside elevated caspase-3 and p62 expression, confirming enhanced apoptosis and autophagy; collectively, the composite demonstrated synergistic anticancer activity mediated by controlled release, ROS amplification, apoptosis induction, and cell cycle arrest [139].

In another study, Babayevska et al. (2025) [140] synthesized crystalline  $Gd_2O_3$  solid spheres ( $Gd_2O_3\_S$ ) and hollow spheres ( $Gd_2O_3\_HS$ ) via soft-chemistry methods, followed by ZnO coating and doxorubicin (Dox) loading, producing annealed solid spheres of ~120 nm (from ~170 nm precursors) and hollow spheres of ~150 nm with tunable shell thicknesses (20–50 nm); BET analysis revealed a higher surface area for  $Gd_2O_3\_HS$  (32.5 m<sup>2</sup>/g) than  $Gd_2O_3\_S$  (15.6 m<sup>2</sup>/g), directly enhancing drug-loading capacity, and upon Dox adsorption, surface areas decreased to 1.9 m<sup>2</sup>/g ( $Gd_2O_3\_S@Dox$ ) and 12.5 m<sup>2</sup>/g ( $Gd_2O_3\_HS@Dox$ ), confirming successful loading. Drug adsorption was strongly pH- and temperature-dependent, reaching ~15% ( $Gd_2O_3\_S$ ) and ~52% ( $Gd_2O_3\_HS$ ) at pH 7.4 and 37 °C after 24 h, but increasing dramatically under mildly acidic conditions (pH 5.5, 37 °C) to 82.31% and 95.41%, respectively, highlighting the superior performance of hollow structures due to greater internal surface area; controlled release studies over 48 h showed pH-responsive behavior, with cumulative release at pH 7.4 plateauing at ~85% ( $Gd_2O_3\_S$ ) and ~76% ( $Gd_2O_3\_HS$ ) after 24 h, whereas acidic conditions (pH 5.5) resulted in lower release (~50% and ~27% after 48 h), indicating stronger drug retention in hollow spheres. Cytotoxicity assays (1–150 µg/mL, 24 h) demonstrated good biocompatibility of pristine  $Gd_2O_3$  nanospheres toward MSU1.1 fibroblasts and HeLa cells (~70–72% viability only at 150 µg/mL), while ZnO-containing systems exhibited increased toxicity at ≥100 µg/mL due to Zn<sup>2+</sup> release and ROS generation; Dox-loaded hollow spheres (7 mg/mL loading solution) produced enhanced cytotoxicity at 100 µg/mL nanoparticle concentration. Photoluminescence analysis revealed strong visible emissions at 460, 484, 523, and 570 nm (maximum at ~460 nm under 273 nm excitation), supporting bioimaging capability, and confocal microscopy confirmed efficient cellular uptake and intracellular Dox release after 6 h at 50 µg/mL, demonstrating the theranostic potential of ZnO- and Dox-functionalized  $Gd_2O_3$  hollow spheres for combined imaging and targeted cancer therapy [140].

Shirazi et al. reported that 11-amino-acids cyclic peptide, [(WR)<sub>5</sub>C], containing five arginine, five tryptophan, and one cysteine residue was used to generate GdNPs for enhanced intracellular delivery of small molecules and drugs (**Figure 5**). The peptide was synthesized via Fmoc solid-phase chemistry and formed star-shaped Gd nanoparticles of approximately 240–260 nm after simple in situ mixing of aqueous peptide and GdCl<sub>3</sub> solutions. Flow cytometry demonstrated that delivery of a fluorescence-labeled phosphopeptide (F'-GpYEEL, 5 µM) increased approximately six-fold in CCRF-CEM cells after 2 h incubation when combined with 50 µM [(WR)<sub>5</sub>C]-GdNPs compared to the phosphopeptide alone. The system also enhanced chemotherapeutic activity: at 5 µM drug concentration and 50 µM nanoparticle concentration, antiproliferative activity increased by 41% for cisplatin and 18% for carboplatin after 72 h. Drug release experiments using epirubicin showed controlled intracellular release, with about 15% released within 12 h and approximately 60% released by 48 h, demonstrating sustained intracellular drug availability [25].

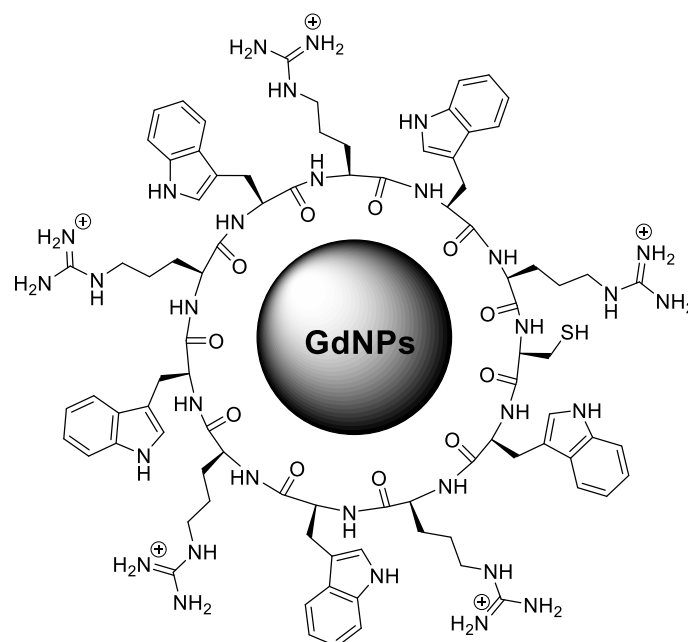


**Figure 5.** Structure of [(WR)<sub>5</sub>C]-GdNPs [25 Shirazi 2020].

In the second study, the same cyclic peptide–Gd system was further optimized and evaluated specifically as an siRNA delivery platform. Star-shaped nanoparticles (240–260 nm) were formed by mixing 1 mM peptide with 1 mM GdCl<sub>3</sub>. Binding analysis using SYBR Green II showed strong affinity for siRNA, with a BC<sub>50</sub> value of 0.044. Zeta potential measurements revealed positive surface charges of +31.7 mV (14 μM) and +36.5 mV (28 μM) for the peptide alone, and +30 mV and +34 mV for the peptide-Gd nanoparticles, enabling efficient complexation with negatively charged siRNA (–15 mV). Cytotoxicity remained low, with approximately 93% cell viability at 50 μM after 48 h in CCRF-CEM and MDA-MB-231 cells. Importantly, fluorescence-activated cell sorting (FACS) showed more than a 10-fold increase in intracellular uptake of Alexa-488-labeled siRNA after 6 h compared to siRNA alone. At an N/P ratio of 40, the nanocomplex achieved approximately 62% reduction of STAT-3 protein expression in MDA-MB-231 cells, confirming effective gene silencing. Together, these studies demonstrate a versatile cyclic peptide–Gd nanoparticle platform capable of enhancing delivery of both small-molecule drugs and nucleic acids with low toxicity and strong intracellular transport efficiency [24].

Wei et al. [141] developed a multifunctional Gd-doped hollow CeO<sub>2</sub>–ZrO<sub>2</sub> nanoplatform (Gd/CeO<sub>2</sub>–ZrO<sub>2</sub>/DOX-PEG) for combined chemotherapy and dual-modal MRI/CT imaging by first synthesizing monodisperse Gd-doped CeO<sub>2</sub> nanospheres (~85 nm) in glycol at 180 °C for 16 h, followed by zirconium incorporation through a Kirkendall effect to generate hollow CeO<sub>2</sub>–ZrO<sub>2</sub> structures with a high BET surface area of 436.7 m<sup>2</sup>/g and mesoporous architecture (pore sizes 3.8 and 13.2 nm); PEGylation increased the hydrodynamic diameter to 120 ± 10 nm and shifted the surface charge to +16.2 mV, confirming successful surface modification. Doxorubicin (DOX) was loaded into the hollow interior with a loading efficiency of 10.2 wt%, and in vitro release studies demonstrated pronounced pH responsiveness, with ~87% DOX released at pH 6.8 (tumor-like acidic conditions) compared with ~30% at physiological pH 7.4, thereby minimizing premature leakage during circulation. The nanoplatform exhibited strong dual-imaging performance, with T<sub>1</sub>-weighted MRI phantom studies at 7.0 T showing concentration-dependent signal enhancement (0–0.9 mM Gd) and a longitudinal relaxivity (r<sub>1</sub>) of 4.63 s<sup>–1</sup>mM<sup>–1</sup>, while CT imaging displayed linear attenuation enhancement (0–4.9 mg/mL) with a slope of ~25.23 HU. In vitro assays confirmed high biocompatibility of empty nanoparticles (>95% HepG-2 viability at 180 μg/mL after 48 h), whereas DOX-loaded nanoparticles induced dose-dependent cytotoxicity, reducing viability to 22.3% at 5 μg/mL DOX after 48 h. In tumor-bearing mice intravenously administered 2.5 mg/kg DOX (seven doses over 22 days), the Gd/CeO<sub>2</sub>–ZrO<sub>2</sub>/DOX-PEG group achieved significantly greater tumor

growth inhibition than free DOX without notable body weight loss, and MRI/CT imaging demonstrated peak tumor enhancement at 4 h post-injection, with MRI gray values increasing from 144.3 to 317.2 and CT values from 40.3 to 76.2 HU, confirming effective tumor accumulation and integrated therapeutic–diagnostic functionality within a single nanostructure [141].

Sun et al. (2024) developed bovine serum albumin-coated gadolinium oxide nanoparticles ( $Gd_2O_3@BSA$ ) as a biocompatible nanocarrier for curcumin (CUR) delivery against nasal squamous cell carcinoma, demonstrating nanoscale stability, pH-responsive release, and strong anticancer efficacy. The nanoparticles were synthesized by mixing 0.25 g BSA with 100 mM  $Gd(NO_3)_3$  under alkaline conditions (pH 12) with 12 h stirring, followed by 48 h dialysis; STEM imaging revealed spherical, monodispersed particles with core sizes below 10 nm, while dynamic light scattering showed a hydrodynamic diameter of 17 nm that increased to 26 nm after CUR loading, confirming successful drug incorporation. The zeta potential shifted from  $-32$  mV to  $-36$  mV upon CUR loading, indicating enhanced colloidal stability, and UV–Vis spectroscopy confirmed encapsulation through characteristic peaks at  $\sim 265$ – $270$  nm ( $Gd_2O_3/BSA$ ) and a broad CUR absorption band around 430 nm; the drug loading content reached 21.3%. In vitro release studies demonstrated pH-sensitive behavior, with  $\sim 65\%$  CUR released within 10 h at pH 4.0 compared to 43% at pH 7.4, followed by sustained release up to 40 h, supporting preferential drug release in acidic tumor-like environments. Biocompatibility assessments showed excellent safety, with hemolysis below 3% even at  $520$   $\mu g/mL$  and nearly 100% viability of normal HFF-2 fibroblasts after 24 h exposure ( $32.5$ – $520$   $\mu g/mL$ ), whereas dose-dependent anticancer activity was observed in CNE-1 and RPMI 2650 carcinoma cells; treatment with  $Gd_2O_3@BSA$ -CUR ( $7.5$ – $120$   $\mu g/mL$ ) resulted in significantly greater cytotoxicity than free CUR, achieving robust tumor cell growth inhibition at  $120$   $\mu g/mL$ , while the blank carrier exhibited minimal toxicity. In vivo evaluation in BALB/c mice administered 25, 50, and 100 mg/kg showed no mortality, no abnormal weight changes, and no histopathological damage in major organs, confirming favorable systemic biocompatibility [142].

## 5. GdNPs in Cancer Therapy

Beyond their role in energy-mediated therapies, GdNPs have been shown to disrupt DNA function and inhibit cancer cell proliferation through multiple mechanisms. GdNPs can interfere with DNA repair pathways, increase oxidative stress, and potentiate radiation-induced double-strand breaks, ultimately leading to cell cycle arrest and apoptosis [143,144].

GdNPs have attracted growing interest as anticancer agents in drug delivery systems due to their ability to interfere with DNA function and suppress cancer cell proliferation [116,145]. Owing to Gd's high atomic number and paramagnetic properties of Gd, GdNPs can amplify radiation-induced DNA damage when used alone or in combination with radiotherapy [119,144]. Upon cellular internalization, these nanoparticles preferentially accumulate in the cytoplasm and nucleus, where they promote the generation of ROS either intrinsically or under external stimuli such as X-ray or photon irradiation [119,134]. Excessive ROS levels induce oxidative stress, leading to DNA single- and double-strand breaks, base modifications, and chromosomal instability, which disrupt DNA replication and transcription [146,147]. These molecular events ultimately trigger cell-cycle arrest and apoptosis in cancer cells while sparing surrounding healthy tissue when appropriate targeting strategies are employed [132,145].

Beyond indirect DNA damage, GdNPs can be engineered to interact more directly with genetic material or DNA-associated proteins. Surface functionalization by cationic peptides, polymers, or small molecules promotes electrostatic interactions with the negatively charged DNA backbone, facilitating nuclear localization and hindering DNA repair pathways [132]. Multiple studies have shown that GdNPs can antagonize essential DNA repair enzymes such as those required for homologous recombination and non-homologous end joining, sensitizing cancer cells to chemotherapeutic drugs and radiation [134,144]. In the context of multifunctional drug delivery platforms, GdNPs are not only active vehicles for cytotoxic drugs or gene-silencing drugs but also act as adjunctive agents against DNA integrity and cancer cell proliferation [147]. Such dual

characteristics as therapeutic enhancement and intrinsic genotoxic stress render GdNPs as promising materials for next-generation anti-cancer nanomedicine.

The ability of GdNPs to disturb DNA function and inhibit cancer cell proliferation directly enhances their effectiveness as drug delivery agents through several synergistic mechanisms. One of the most significant contributions is sensitization of tumor cells to co-delivered therapeutics. GdNPs can promote the generation of ROS, either intrinsically or under external stimulation such as X-ray or photon irradiation, leading to DNA single- and double-strand breaks and replication stress [116,119]. These genotoxic effects commonly induce cell-cycle arrest at the G2/M phase, a stage at which cancer cells are particularly sensitive to chemotherapy and radiotherapy [148 Pawlik 2004]. Consequently, drugs delivered in combination with GdNPs exhibit enhanced cytotoxicity, enabling reduced drug dosages while limiting systemic toxicity.

In addition, the DNA-disturbing properties of GdNPs improve intracellular drug retention and nuclear delivery. Activation of DNA damage response pathways results in chromatin remodeling and altered nuclear membrane dynamics, thereby increasing nuclear permeability and retention of nanoparticle-associated payloads [146]. Surface-engineered GdNPs functionalized with cationic polymers, peptides, or targeting ligands can further enhance electrostatic interactions with the negatively charged DNA backbone, promoting nuclear accumulation of both the nanoparticles and their therapeutic cargo [132]. This characteristic could be especially beneficial for DNA-targeting agents, including platinum-based drugs, topoisomerase inhibitors, and gene-regulating therapeutics, as it increases drug–DNA proximity and therapeutic efficiency. Finally, the intrinsic ability of GdNPs to interfere with DNA repair pathways enables them to function as active drug delivery systems rather than passive carriers. GdNPs have been shown to inhibit key DNA repair mechanisms, including homologous recombination and non-homologous end joining, thereby preventing cancer cells from recovering from therapy-induced DNA damage [145 Her, 2017; 147 Wang 2018]. This suppression of DNA repair could reduce the emergence of drug resistance and enhances apoptosis when GdNPs are combined with chemotherapy, radiotherapy, or gene therapy.

Gadolinium nanoparticles (GdNPs) can enhance drug delivery by co-transporting therapeutic agents, biologically priming cancer cells for amplified therapeutic responses, and simultaneously providing MRI contrast, as demonstrated by Zhang et al., who developed Gd<sup>3+</sup>-doped MgAl layered double hydroxide (Gd-LDH) nanosheets as a combined drug delivery and imaging platform via a coprecipitation method yielding particles with a Mg:Al:Gd molar ratio of approximately 2.1:1:0.05 and an initial hydrodynamic size of  $186 \pm 1$  nm; anticancer drugs were incorporated through ion exchange (400 mg LDH mixed with 390 mg 5-fluorouracil (5FU) or 455 mg methotrexate (MTX) at pH 9.5 for 48 h), increasing particle sizes to  $303 \pm 4$  nm (5FU) and  $416 \pm 4$  nm (MTX), confirming successful loading, with higher drug loading observed for MTX ( $34.6 \pm 5.9$  wt%, ~30% encapsulation efficiency) compared to 5FU ( $13.2 \pm 6.2$  wt%, ~13% efficiency); structural analyses revealed expanded interlayer spacing and FTIR-confirmed drug incorporation within LDH layers. Drug release exhibited clear pH responsiveness, with MTX release reaching ~80% at pH 5.0, 67% at pH 6.5, and 57% at pH 7.4 after 48 h, while 5FU release reached ~88%, 75%, and 70% at the respective pH values, with ~70% released within the first 2 h via diffusion and ion exchange; stability studies showed negligible Gd release at physiological pH 7.4 and only 1.9–2.9% leaching under acidic conditions after 24 h. Notably, pristine Gd-LDH exhibited high longitudinal relaxivity ( $r_1 = 9.5 \pm 1.2$  mM<sup>-1</sup>s<sup>-1</sup>), approximately double that of the clinical agent Gd(DTPA) ( $4.5 \pm 0.6$  mM<sup>-1</sup>s<sup>-1</sup>), and although relaxivity decreased at neutral pH ( $\sim 0.83$  mM<sup>-1</sup>s<sup>-1</sup>) after drug loading, it increased under acidic conditions to 2.3–2.7 mM<sup>-1</sup>s<sup>-1</sup> over 24 h, highlighting the system's high drug-loading capacity, controlled pH-sensitive release, physiological stability, and effective MRI contrast performance [50].

## 6. Future Perspectives

A clear near-term direction is the design of ultrasmall, renal-clearable and/or biodegradable GdNPs that preserve high relaxivity, while minimizing long-term retention, an especially important translational consideration given ongoing regulatory and clinical attention to Gd retention and GBCA

safety. Recent practice guidance continues to emphasize risk stratification, differences across agent classes, and patient-specific considerations (e.g., renal function), reinforcing the need for next-generation GdNPs with predictable clearance and robust kinetic stability [149].

GdNPs are poised to evolve from “contrast-enabled carriers” into active, therapeutic nanomedicines that integrate delivery, local energy deposition, and real-time treatment monitoring. Beyond MRI, the most impactful expansion of GdNPs is likely in energy-enabled theranostics, where Gd’s high atomic number and magnetic behavior are leveraged to amplify therapy at the disease site while imaging confirms delivery. In oncology, GdNPs are being advanced as radiosensitizers and as multifunctional systems that can pair MRI guidance with radiation enhancement and drug release; hybrid compositions (including high-Z architectures and engineered surface chemistries) are also being explored to improve therapeutic gain under clinically relevant irradiation conditions [117,118]. In parallel, GdNP-enabled neutron capture therapy (Gd-NCT) and cell-assisted delivery concepts (e.g., for glioblastoma targeting) represent a route to overcome rapid clearance and nonspecific biodistribution, which have historically limited Gd-based approaches in these settings [111,119].

From a drug-delivery standpoint, future GdNP platforms will likely emphasize programmable biointeractions: (i) stealth-to-adhesive or charge-reversible surfaces that circulate neutrally yet switch to cationic/interactive states within acidic or enzyme-rich microenvironments; (ii) organelle-targeted systems (nucleus/mitochondria/lysosome) to synchronize payload localization with Gd-mediated radiosensitization or ROS stress; and (iii) multi-cargo formulations (drug + immunomodulator + imaging function) to enable treatment sequencing and adaptive dosing. These strategies align with broader trends favoring sub-15 nm constructs for improved tissue penetration and more favorable clearance profiles, while still enabling sufficient payload capacity via high-affinity conjugation chemistries and porous/hybrid architectures [73,93,94].

Clinical translation will ultimately depend on addressing “engineering-to-regulation” gaps: scalable synthesis with tight control of hydrodynamic size distribution, batch-to-batch relaxivity, and leachable/free Gd<sup>3+</sup>; standardized assays for speciation and long-term fate; and harmonized safety packages that address retention, immunotoxicology, reproductive safety, and special populations. The late-stage progress of new, higher-relaxivity macrocyclic agents such as gadopentate demonstrates an industry-wide push toward higher imaging efficiency per Gd dose and may indirectly shape expectations for GdNP products. Future approvals will likely favor platforms that can demonstrate both superior performance and a compelling risk–benefit profile grounded in clearance, stability, and monitoring [113].

## 7. Conclusions

GdNPs developed from being modified for MRI contrast enhancement to multifunctional nanoparticles with broad applications in drug delivery and theranostics. Their special electronic configuration, high atomic number, and flexible coordination chemistry facilitate the simultaneous imaging, radiosensitization, photothermal enhancement, and controlled therapeutic delivery. In contrast to traditional low–molecular-weight Gd chelates, nanoscale formulation has tunable size, surface charge, and ligand structure and they feature an optimal control in pharmacokinetics, biodistribution, and tumor targeting. Such property situate GdNPs as versatile platform materials that have the potential in unifying diagnosis and therapy under one construct.

Therapeutically, GdNPs offer synergistic benefits with chemotherapy, radiotherapy and novel energy-based modalities. This ability to amplify radiation-induced DNA damage, produce ROS, and modulate intracellular stress pathways, which would increase anticancer efficacy but reduce the delivery of the cytotoxic agents, through the presence of other targeted cytotoxic agents, is critical due to their potential for potentiation of the pathways. Engineering the surface, such as PEGylation, peptide conjugation and stimulus-responsive coatings, that enhance tumor selectivity and reduce the systemic toxicity is not only made possible by such surface engineering methodologies as PEGylation, peptide conjugation and stimulus-responsive coatings but also minimizes the tumor-traction. Crucially, the intrinsic MRI visibility of Gd allows for the up-to-the-minute tracking of the

nanoparticle biodistribution in the body, a valuable technology in time sensitive drug planning, response monitoring and treatment response monitoring with personalized tailor-made clinical management of Gd. Despite the success at preclinical trials at preclinical stage, multiple translational hurdles still exist. Long-term Gd retention, speciation, and potential toxicity concerns further highlight the importance of ultrasmall, biodegradable, and kinetically stable formulations with predictable pathways of clearance. Regulatory approval will depend on systematic assessment of pharmacokinetics, tissue deposition/transformation, and immune compatibility. In addition, scalable and reproducible manufacturing means need to be set up to ensure batch consistency, structural integrity and controlled drug loading at clinically-relevant scales. GdNPs represent a compelling frontier in precision nanomedicine. Continued advances in materials chemistry, surface functionalization, and multimodal integration are expected to expand their utility beyond imaging into fully integrated therapeutic systems. With careful attention to safety, biodegradability, and regulatory considerations, GdNP-based platforms hold strong promise for the development of next-generation image-guided drug delivery systems and personalized theranostic strategies in oncology and beyond.

**Author Contributions:** A.N.S. prepared the initial manuscript draft; A.K., K.P., R.V., H.Z., and P.M. revised the text and provided guidance. All authors have read and agreed to the published version of the manuscript.

**Funding:** This work received no external funding.

**Acknowledgments:** The authors acknowledge financial support from Marshall B. Ketchum University, College of Pharmacy, Fullerton, CA, Chapman University School of Pharmacy, and NIH grant no. 1R15CA301437-01. ChatGPT5.2 was used to reformat the references and edit the text.

**Conflicts of Interest:** The authors declare no conflicts of interest.

## Abbreviations

The following abbreviations are used in this manuscript:

GdNPS	Gadolinium Nanoparticles
REEs	Rare Earth Elements
ADME	Absorption, Distribution, Metabolism, and Excretion

## References

1. Shirazi, A.N.; Vadlapatla, R.; Koomer, A.; Nguyen, A.; Khoury, V.; Parang, K. Peptide-Based Inorganic Nanoparticles as Efficient Intracellular Delivery Systems. *Pharmaceutics* **2025**, *17*, 1123.
2. Salavati-Niasari, M.; Davar, F.; Mir, N. Synthesis and Characterization of Metallic Copper Nanoparticles via Thermal Decomposition. *Polyhedron* **2008**, *27*, 3514–3518.
3. Ealia, S.A.M.; Saravanakumar, M.P. A Review on the Classification, Characterisation, Synthesis of Nanoparticles and Their Application. *IOP Conf. Ser. Mater. Sci. Eng.* **2017**, *263*, 032019.
4. Kim, H.; Mondal, S.; Jang, B.; Manivasagan, P.; Moorthy, M.S.; Oh, J. Biomimetic Synthesis of Metal-Hydroxyapatite (Au-HAp, Ag-HAp, Au-Ag-HAp): Structural Analysis, Spectroscopic Characterization and Biomedical Application. *Ceram. Int.* **2018**, *44*, 20490–20500.
5. Iravani, S. Green Synthesis of Metal Nanoparticles Using Plants. *Green Chem.* **2011**, *13*, 2638–2650.
6. Khan, M.U.; Ullah, H.; Honey, S.; Talib, Z.; Abbas, M.; Umar, A.; Ahmad, T.; Sohail, J.; Sohail, A.; Makgopa, K.; et al. Metal Nanoparticles: Synthesis Approach, Types and Applications—A Mini Review. *Nano-Horizons* **2023**, *2*, 1–21.
7. Chakraborty, I.; Pradeep, T. Atomically Precise Clusters of Noble Metals: Emerging Link between Atoms and Nanoparticles. *Chem. Rev.* **2017**, *117*, 8208–8271.
8. Zaleska-Medynska, A.; Marchelek, M.; Diak, M.; Grabowska, E. Noble Metal-Based Bimetallic Nanoparticles: The Effect of the Structure on the Optical, Catalytic and Photocatalytic Properties. *Adv. Colloid Interface Sci.* **2016**, *229*, 80–107.

9. Vasić, K.; Knez, Ž.; Leitgeb, M. Multifunctional Iron Oxide Nanoparticles as Promising Magnetic Biomaterials in Drug Delivery: A Review. *J. Funct. Biomater.* **2024**, *15*, 227.
10. Karim, W.; Kleibert, A.; Hartfelder, U.; Bansmann, J.; Bäumer, M. Size-Dependent Redox Behavior of Iron Observed by In-Situ Single Nanoparticle Spectro-Microscopy on Well-Defined Model Systems. *Sci. Rep.* **2016**, *6*, 18818
11. Tai, C.Y.; Tai, C.-T.; Chang, M.-H.; Liu, H.-S. Synthesis of Magnesium Hydroxide and Oxide Nanoparticles Using a Spinning Disk Reactor. *Ind. Eng. Chem. Res.* **2007**, *46*, 5536–5541.
12. Vargas-Ortiz, J.R.; Gonzalez, C.; Esquivel, K. Magnetic Iron Nanoparticles: Synthesis, Surface Enhancements, and Biological Challenges. *Processes* **2022**, *10*, 2282.
13. Le, N.; Zhang, M.; Kim, K. Quantum Dots and Their Interaction with Biological Systems. *Int. J. Mol. Sci.* **2022**, *23*, 10763.
14. Iravani, S.; Korbekandi, H.; Mirmohammadi, S.V.; Zolfaghari, B. Synthesis of Silver Nanoparticles: Chemical, Physical and Biological Methods. *Res. Pharm. Sci.* **2014**, *9*, 385–406.
15. Gupta, A.K.; Gupta, M. Synthesis and Surface Engineering of Iron Oxide Nanoparticles for Biomedical Applications. *Biomaterials* **2005**, *26*, 3995–4021.
16. Genc, S.; Taghizadehghalehjoughi, A.; Yeni, Y.; Jafarizad, A.; Hacimuftuoglu, A.; Nikitovic, D.; Docea, A.O.; Mezhev, Y.; Tsatsakis, A. Fe<sub>3</sub>O<sub>4</sub> Nanoparticles in Combination with 5-FU Exert Antitumor Effects Superior to Those of the Active Drug in a Colon Cancer Cell Model. *Pharmaceutics* **2023**, *15*, 245.
17. Premanathan, M.; Karthikeyan, K.; Jeyasubramanian, K.; Manivannan, G. Selective Toxicity of ZnO Nanoparticles toward Gram-Positive Bacteria and Cancer Cells by Apoptosis through Lipid Peroxidation. *Nanomedicine* **2011**, *7*, 184–192.
18. Chen, G.; Yang, F.; Fan, S.; Jin, H.; Liao, K.; Li, X.; Liu, G.B.; Liang, J.; Zhang, J.; Xu, J.F.; et al. Immunomodulatory Roles of Selenium Nanoparticles: Novel Arts for Potential Immunotherapy Strategy Development. *Front. Immunol.* **2022**, *13*, 956181.
19. Huang, Y.; He, L.; Liu, W.; Fan, C.; Zheng, W.; Wong, Y.S.; Chen, T. Selective Cellular Uptake and Induction of Apoptosis of Cancer-Targeted Selenium Nanoparticles. *Biomaterials* **2013**, *34*, 7106–7116.
20. Gong, G.; Fu, B.; Ying, C.; Zhu, Z.; He, X.; Li, Y.; Shen, Z.; Xuan, Q.; Huang, Y.; Lin, Y.; et al. Targeted Delivery of Paclitaxel by Functionalized Selenium Nanoparticles for Anticancer Therapy through ROS-Mediated Signaling Pathways. *RSC Adv.* **2018**, *8*, 39957–39966.
21. Caravan, P.; Ellison, J.J.; McMurry, T.J.; Lauffer, R.B. Gadolinium(III) Chelates as MRI Contrast Agents: Structure, Dynamics, and Applications. *Chem. Rev.* **1999**, *99*, 2293–2352.
22. Lauffer, R.B. Paramagnetic Metal Complexes as Water Proton Relaxation Agents for NMR Imaging. *Chem. Rev.* **1987**, *87*, 901–927.
23. Wang, H.; Liu, Y.; Zhang, M.; Wang, J.; Wu, Z.; Li, L. Gadolinium-Based Nanoparticles for Theranostic Applications: A Review. *ACS Appl. Nano Mater.* **2021**, *4*, 4673–4691.
24. Shirazi, A.N.; Sajid, M.I.; Mandal, D.; Stickley, D.; Nagasawa, S.; Long, J.; Lohan, S.; Parang, K.; Tiwari, R.K. Cyclic Peptide-Gadolinium Nanocomplexes as siRNA Delivery Tools. *Pharmaceutics* **2021**, *14*, 1064.
25. Shirazi, A.N.; Park, S.E.; Rad, S.; Baloyan, L.; Mandal, D.; Sajid, M.I.; Hall, R.; Lohan, S.; Zoghebi, K.; Parang, K.; et al. Cyclic Peptide-Gadolinium Nanoparticles for Enhanced Intracellular Delivery. *Pharmaceutics* **2020**, *12*, 792.
26. Shirazi, A.N.; Paquin, K.L.; Howlett, N.G.; Mandal, D.; Parang, K. Cyclic Peptide-Capped Gold Nanoparticles for Enhanced siRNA Delivery. *Molecules* **2014**, *19*, 13319–13331.
27. Nasrolahi Shirazi, A.; Tiwari, R.K.; Oh, D.; Sullivan, B.; McCaffrey, K.; Mandal, D.; Parang, K. Surface Decorated Gold Nanoparticles by Linear and Cyclic Peptides as Molecular Transporters. *Mol. Pharm.* **2013**, *10*, 3137–3146.
28. Nasrolahi Shirazi, A.; Mandal, D.; Tiwari, R.K.; Guo, L.; Lu, W.; Parang, K. Cyclic Peptide-Capped Gold Nanoparticles as Drug Delivery Systems. *Mol. Pharm.* **2013**, *10*, 500–508.
29. Shirazi, A.N.; Vadlapatla, R.; Koomer, A.; Yep, K.; Parang, K. Selenium Nanoparticles as Versatile Delivery Tools. *Pharmaceutics* **2025**, *17*, 1556.
30. Greenwood, N.N.; Earnshaw, A. *Chemistry of the Elements*, 2nd ed.; Butterworth-Heinemann: Oxford, UK, **1997**; pp. 1227–1249.

31. Pyykkö, P. Magically Magnetic Gadolinium. *Nat. Chem.* **2015**, *7*, 680–681.
32. Abragam, A.; Bleaney, B. *Electron Paramagnetic Resonance of Transition Ions*; Oxford University Press: Oxford, UK, 2012.
33. Laing, M. Gadolinium: Central Metal of the Lanthanoids. *J. Chem. Educ.* **2009**, *86*, 188–189.
34. Araj, S.; Colvin, R.V. Magnetic Susceptibility of Gadolinium, Terbium, and Dysprosium Metals. *J. Appl. Phys.* **1961**, *32*(3), S336–S337.
35. Robertson, A.G.; Rendina, L.M. Gadolinium Theranostics for the Diagnosis and Treatment of Cancer. *Chem. Soc. Rev.* **2021**, *50*, 4231–4244.
36. Ramalho, J.; Semelka, R.C.; Ramalho, M.; Nunes, R.H.; AlObaidy, M.; Castillo, M. Gadolinium-Based Contrast Agent Accumulation and Toxicity: An Update. *AJNR Am. J. Neuroradiol.* **2016**, *37*, 1192–1198.
37. Liu, Y.; Tegafaw, T.; Baek, A.; Ho, S.L.; Zhao, D.; Chen, X.; Mulugeta, E.; Lee, H.; Nam, H.; Kim, J.; Chang, Y.; Lee, G.H. Tumor-Targeting T<sub>1</sub> MRI Contrast Agents with Antioxidant Effects: Gadolinium Oxide Nanoparticles Grafted with Polydopamine- and Polyserotonin-Conjugated Polyacrylic Acids. *ACS Omega* **2025**, *10*, 58885–58899.
38. Bashir, A.; Gray, M.L.; Burstein, D. Gd-DTPA<sup>2-</sup> as a measure of cartilage degradation. *Magn. Reson. Med.* **1996**, *36*(5), 665–673.
39. Nieminen, M.T.; Rieppo, J.; Silvennoinen, J.; Töyräs, J.; Hakumäki, J.M.; Hyttinen, M.M.; Helminen, H.J.; Jurvelin, J.S. Spatial assessment of articular cartilage proteoglycans with Gd-DTPA-enhanced T<sub>1</sub> imaging. *Magn. Reson. Med.* **2002**, *48*(4), 640–648.
40. Miyata, S.; Homma, K.; Numano, T.; Furukawa, K.; Tateishi, T.; Ushida, T. Assessment of fixed charge density in regenerated cartilage by Gd-DTPA-enhanced MRI. *Magn. Reson. Med. Sci.* **2006**, *5*, 73–78.
41. Chen, C.T.; Fishbein, K.W.; Torzilli, P.A.; Hilger, A.; Spencer, R.G.; Horton, W.E., Jr. Matrix fixed-charge density as determined by magnetic resonance microscopy of bioreactor-derived hyaline cartilage correlates with biochemical and biomechanical properties. *Arthritis Rheum.* **2003**, *48*(4), 1047–1056.
42. Ogan, M.D.; Schmiedl, U.; Moseley, M.E.; Grodd, W.; Paajanen, H.; Brasch, R.C. Albumin labeled with Gd-DTPA. An intravascular contrast-enhancing agent for magnetic resonance blood pool imaging: Preparation and characterization. *Invest. Radiol.* **1987**, *22*(8), 665–671.
43. Li, L.; Jiang, W.; Luo, K.; Song, H.; Lan, F.; Wu, Y.; Gu, Z. Superparamagnetic Iron Oxide Nanoparticles as MRI Contrast Agents for Non-Invasive Stem Cell Labeling and Tracking. *Theranostics* **2013**, *3*(8), 595–615.
44. Parfenov, V.A.; Koudan, E.V.; Bulanova, E.A.; Karalkin, P.A.; DAS Pereira, F.; Norkin, N.E.; Knyazeva, A.D.; Gryadunova, A.A.; Petrov, O.F.; Vasiliev, M.M.; Myasnikov, M.I.; Chernikov, V.P.; Kasyanov, V.A.; Marchenkov, A.Y.; Brakke, K.; Khesuani, Y.D.; Demirci, U.; Mironov, V.A. Scaffold-Free, Label-Free and Nozzle-Free Biofabrication Technology Using Magnetic Levitational Assembly. *Biofabrication* **2018**, *10*, 034104.
45. Parfenov, V.A.; Mironov, V.A.; Koudan, E.V.; Nezhurina, E.K.; Karalkin, P.A.; Pereira, F.D.A.S.; Petrov, S.V.; Krokmal, A.A.; Aydemir, T.; Vakhrushev, I.V.; Zobkov, Y.V.; Smirnov, I.V.; Fedotov, A.Y.; Demirci, U.; Khesuani, Y.D.; Komlev, V.S. Fabrication of Calcium Phosphate 3D Scaffolds for Bone Repair Using Magnetic Levitational Assembly. *Sci. Rep.* **2020**, *10*, 4013.
46. Türker, E.; Demirçak, N.; Arslan-Yildiz, A. Scaffold-free three-dimensional cell culturing using magnetic levitation. *Biomater. Sci.* **2018**, *6*, 1745–1753.
47. Pan, X.; Hu, M.; Wu, L.; Wei, E.; Zhu, Q.; Lv, L.; Xv, X.; Dong, X.; Liu, H.; Liu, Y. Biomedical Applications of Gadolinium-Containing Biomaterials: Not Only MRI Contrast Agent. *Adv. Sci.* **2025**, *12*, e2501722.
48. Kroklicheva, P.A.; Goldberg, M.A.; Fomin, A.S.; Khayrutdinova, D.R.; Antonova, O.S.; Sadovnikova, M.A.; Mikheev, I.V.; Leonov, A.V.; Merzlyak, E.M.; Kovalishina, D.A.; Akhmedova, S.A.; Sergeeva, N.S.; Gafurov, M.R.; Barinov, S.M.; Komlev, V.S. Gadolinium-Doped Injectable Magnesium-Calcium Phosphate Bone Cements for Noninvasive Visualization. *J. Magnes. Alloys* **2024**, *12*, 3698–3716.
49. Chaturvedi, K.; Singhwani, A.; Jaiswal, A.; Mili, M.; Tilwari, A.; Mohapatra, R.K.; Srivastava, A.K.; Verma, S. Robust Synthesis and Characteristics of Novel One-Dimensional Gadolinium Oxide Nanorods Decorated Multiwalled Carbon Nanotubes Based Antibacterial Nanocomposites for Health Care Applications. *Inorg. Chem. Commun.* **2023**, *157*, 111324.

50. Zhang, Z.; Wells, C.J.R.; Liang, R.; et al. Gadolinium Doped Layered Double Hydroxides for Simultaneous Drug Delivery and Magnetic Resonance Imaging. *J. Clust. Sci.* **2023**, *34*, 385–394.
51. Zhang, J.; Lu, L.; Zhang, W.; Miao, Y.; Du, H.; Xia, H.; Tao, Z.; Du, Z.; Tang, Y.; Fang, Q. Gadolinium Ion-Loaded Mesoporous Organosilica NanoplatforM for Enhanced Radiotherapy in Breast Tumor Treatment. *Colloids Surf. B Biointerfaces* **2025**, *246*, 114374.
52. Sun, Z.; Zhou, Y.; Li, L.; Zhou, C.; Jia, W.; Liu, Y.; Cao, X.; Su, S.; Zhao, Z.; Zhen, M.; Wang, C. Gadolinium-Based Nanomaterials for Advanced Biomedical Applications. *Sci. Bull.* **2023**, *68*, 1651–1665.
53. Mulugeta, E.; Tegafaw, T.; Liu, Y.; Zhao, D.; Chen, X.; Baek, A.; Kim, J.; Chang, Y.; Lee, G.H. Current Status and Future Aspects of Gadolinium Oxide Nanoparticles as Positive Magnetic Resonance Imaging Contrast Agents. *Nanomaterials* **2025**, *15*, 1340.
54. Pecharsky, V.K.; Gschneidner, K.A., Jr. Magnetocaloric Effect and Magnetic Refrigeration. *J. Magn. Magn. Mater.* **1999**, *200*, 44–56.
55. Blomqvist, L.; Nordberg, G.F.; Nurchi, V.M.; Aaseth, J.O. Gadolinium in Medical Imaging—Usefulness, Toxic Reactions and Possible Countermeasures—A Review. *Biomolecules* **2022**, *12*, 742.
56. Henderson, I.M.; Benevidez, A.D.; Mowry, C.D.; Watt, J.; Bachand, G.D.; Kirk, M.L.; Dokładny, K.; DeAgüero, J.; Escobar, G.P.; Wagner, B. Precipitation of gadolinium from magnetic resonance imaging contrast agents may be the brass tacks of toxicity. *Magn. Reson. Imaging* **2025**, *119*, 110383.
57. McDonald, R.J.; McDonald, J.S.; Kallmes, D.F.; Jentoft, M.E.; Murray, D.L.; Thielen, K.R.; Williamson, E.E.; Eckel, L.J. Intracranial Gadolinium Deposition after Contrast-Enhanced MR Imaging. *Radiology* **2015**, *275*(3), 772–782.
58. Kanda, T.; Ishii, K.; Kawaguchi, H.; Kitajima, K.; Takenaka, D. High Signal Intensity in the Dentate Nucleus and Globus Pallidus on Unenhanced T1-Weighted MR Images: Relationship with Increasing Cumulative Dose of a Gadolinium-Based Contrast Material. *Radiology* **2014**, *270*(3), 834–841.
59. Diagaradjane, P.; Deorukhkar, A.; Gelovani, J.G.; Maru, D.M.; Krishnan, S. Gadolinium Chloride Augments Tumor-Specific Imaging of Targeted Quantum Dots In Vivo. *ACS Nano* **2010**, *4*(7), 4131–4141.
60. Faucher, L.; Guay-Bégin, A.-A.; Lagueux, J.; Côté, M.-F.; Petitclerc, É.; Fortin, M.-A. Ultra-Small Gadolinium Oxide Nanoparticles to Image Brain Cancer Cells In Vivo with MRI. *Contrast Media Mol. Imaging* **2011**, *6*, 209–218.
61. Jiang, X.; Mietner, J.B.; Raveendran, D.; Ovchinnikov, K.V.; Sochor, B.; Mueller, S.; Boehm-Sturm, P.; Lerouge, F.; Chaput, F.; Gurikov, P.; Roth, S.V.; Navarro, J.R.G. Multifunctional Cellulose Nanofibrils-GdF<sub>3</sub> Nanoparticles Hybrid Gel and Its Potential Uses for Drug Delivery and Magnetic Resonance Imaging. *ACS Appl. Nano Mater.* **2023**, *6*, 21182–21193.
62. Vecchione, D.; Aiello, M.; Cavaliere, C.; Nicolai, E.; Netti, P.A.; Torino, E. Hybrid Core-Shell Nanoparticles Entrapping Gd-DTPA and <sup>18</sup>F-FDG for Simultaneous PET/MRI Acquisitions. *Nanomedicine* **2017**, *12*, 2223–2231.
63. Fauzia, R.P.; Afriani, Z.; Haryuni, R.D.; Juliyanto, S.; Wyantuti, S.; Bahti, H.H. Effect of Size, Charge, and Surface Functionalization of Gadolinium Nanoparticles on Biocompatibility and Cellular Uptake as Magnetic Resonance Imaging Contrast Agents. *Trends Sci.* **2025**, *22*, 9330.
64. Zhu, D.; Liu, F.; Ma, L.; Liu, D.; Wang, Z. Nanoparticle-Based Systems for T1-Weighted Magnetic Resonance Imaging Contrast Agents. *Int. J. Mol. Sci.* **2013**, *14*, 10591–10607.
65. Liu, Y.; Zhang, N. Gadolinium-Loaded Nanoparticles in Theranostic Magnetic Resonance Imaging. *Biomaterials* **2012**, *33*(21), 5363–5375.
66. Šimečková, P.; Hubatka, F.; Kotouček, J.; et al. Gadolinium Labelled Nanoliposomes as the Platform for MRI Theranostics: In Vitro Safety Study in Liver Cells and Macrophages. *Sci. Rep.* **2020**, *10*, 4780.
67. Tran, V.-L.; Thakare, V.; Natuzzi, M.; Moreau, M.; Oudot, A.; Vrigneaud, J.M.; Courteau, A.; Louis, C.; Roux, S.; Boschetti, F.; Denat, F.; Tillement, O.; Lux, F. Functionalization of Gadolinium Chelates Silica Nanoparticle through Silane Chemistry for Simultaneous MRI/<sup>64</sup>Cu PET Imaging. *Contrast Media Mol. Imaging* **2018**, *2018*, 7938267.
68. Karati, D.; Meur, S.; Roy, S.; Mukherjee, S. Gadolinium Based NanoplatforM as Drug Delivery Approach for Targeted Therapy. *J. Drug Deliv. Sci. Technol.* **2026**, *115*, 107807.

69. Yong, Y.; Zhou, L.; Zhang, S.; et al. Gadolinium Polytungstate Nanoclusters: A New Theranostic with Ultrasmall Size and Versatile Properties for Dual-Modal MR/CT Imaging and Photothermal Therapy/Radiotherapy of Cancer. *NPG Asia Mater.* **2016**, *8*, e273.
70. Dutta Gupta, Y.; Mackeyev, Y.; Krishnan, S.; et al. Mesoporous Silica Nanotechnology: Promising Advances in Augmenting Cancer Theranostics. *Cancer Nanotechnol.* **2024**, *15*, 9.
71. Domingo, J.L.; Semelka, R.C. Gadolinium Toxicity: Mechanisms, Clinical Manifestations, and Nanoparticle Role. *Arch. Toxicol.* **2025**, *99*, 3897–3916.
72. Sancey, L.; Kotb, S.; Truillet, C.; Appaix, F.; Marais, A.; Thomas, E.; van der Sanden, B.; Klein, J.-P.; Laurent, B.; Cottier, M.; Antoine, R.; Dugourd, P.; Panczer, G.; Lux, F.; Perriat, P.; Motto-Ros, V.; Tillement, O. Long-Term In Vivo Clearance of Gadolinium-Based AGuIX Nanoparticles and Their Biocompatibility after Systemic Injection. *ACS Nano* **2015**, *9*, 2477–2488.
73. Fatima, A.; Ahmad, M.W.; Al Saidi, A.K.A.; Choudhury, A.; Chang, Y.; Lee, G.H. Recent Advances in Gadolinium Based Contrast Agents for Bioimaging Applications. *Nanomaterials* **2021**, *11*, 2449.
74. Lux, F.; Sancey, L.; Bianchi, A.; Crémillieux, Y.; Roux, S.; Tillement, O. Gadolinium-Based Nanoparticles for Theranostic MRI-Radiosensitization. *Nanomedicine* **2015**, *10*, 1801–1815.
75. Liu, Y.; Ai, K.; Lu, L. Nanoparticulate Gadolinium Complexes as MRI Contrast Agents. *Chem. Rev.* **2014**, *114*, 5057–5115.
76. Rowe, M.D.; Thamm, D.H.; Kraft, S.L.; Boyes, S.G. Polymer-Modified Gadolinium Metal-Organic Framework Nanoparticles Used as Multifunctional Nanomedicines for the Targeted Imaging and Treatment of Cancer. *Biomacromolecules* **2009**, *10*, 983–993.
77. Khajuria, H.; Ladol, J.; Singh, R.; Khajuria, S.; Khajuria, H.N. Surfactant Assisted Sonochemical Synthesis and Characterization of Gadolinium Doped Zinc Oxide Nanoparticles. *Acta Chim. Slov.* **2015**, *62*, 849–858.
78. Li, Z.; Guo, J.; Zhang, M.; Li, G.; Hao, L. Gadolinium-Coated Mesoporous Silica Nanoparticle for Magnetic Resonance Imaging. *Front. Chem.* **2022**, *10*, 837032.
79. Unruh, C.; Van Bavel, N.; Anikovskiy, M.; Prenner, E.J. Benefits and Detriments of Gadolinium: From Medical Advances to Health and Ecological Risks. *Molecules* **2020**, *25*, 5762.
80. Kotb, S.; Detappe, A.; Lux, F.; Appaix, F.; Barbier, E.L.; Tran, V.-L.; Plissonneau, M.; Gehan, H.; Lefranc, F.; Rodriguez-Lafrasse, C.; Verry, C.; Berbeco, R.; Tillement, O.; Sancey, L. Gadolinium-Based Nanoparticles and Radiation Therapy for Multiple Brain Melanoma Metastases: Proof of Concept before Phase I Trial. *Theranostics* **2016**, *6*, 418–427.
81. Chen, J.S.; Chen, J.; Bhattacharjee, S.; Cao, Z.; Wang, H.; Swanson, S.D.; et al. Functionalized Nanoparticles with Targeted Antibody to Enhance Imaging of Breast Cancer In Vivo. *J. Nanobiotechnol.* **2020**, *18*, 135–139.
82. Usman, M.S.; Hussein, M.Z.; Fakurazi, S.; et al. Gadolinium-Based Layered Double Hydroxide and Graphene Oxide Nano-Carriers for Magnetic Resonance Imaging and Drug Delivery. *Chem. Cent. J.* **2017**, *11*, 47.
83. Truillet, C.; Bouziotis, P.; Tsoukalas, C.; Brugière, J.; Martini, M.; Sancey, L.; Brichart, T.; Denat, F.; Boschetti, F.; Darbost, U.; Bonnamour, I.; Stellas, D.; Anagnostopoulos, C.D.; Koutoulidis, V.; Mouloupoulos, L.A.; Perriat, P.; Lux, F.; Tillement, O. Ultrasmall Particles for Gd-MRI and <sup>68</sup>Ga-PET Dual Imaging. *Contrast Media Mol. Imaging* **2015**, *10*(4), 309–319.
84. Tillement, O.; Lux, F.; Luciani, N.; et al. Gadolinium-Based Nanoparticles for Theranostic MRI. *Adv. Healthc. Mater.* **2014**, *3*, 1769–1782.
85. Lux, F.; Tran, V.L.; Thomas, E.; Dufort, S.; Rossetti, F.; Martini, M.; Truillet, C.; Doussineau, T.; Bort, G.; Denat, F.; Boschetti, F.; Angelovski, G.; Detappe, A.; Crémillieux, Y.; Mignet, N.; Doan, B.-T.; Larrat, B.; Meriaux, S.; Barbier, E.; Roux, S.; Fries, P.; Müller, A.; Abadjian, M.-C.; Anderson, C.; Canet-Soulas, E.; Bouziotis, P.; Barberi-Heyob, M.; Frochot, C.; Verry, C.; Balosso, J.; Evans, M.; Sidi-Boumedine, J.; Janier, M.; Butterworth, K.; McMahan, S.; Prise, K.; Aloy, M.-T.; Ardail, D.; Rodriguez-Lafrasse, C.; Porcel, E.; Lacombe, S.; Berbeco, R.; Allouch, A.; Perfettini, J.-L.; Chargari, C.; Deutsch, E.; Le Duc, G.; Tillement, O. AGuIX® from Bench to Bedside—Transfer of an Ultrasmall Theranostic Gadolinium-Based Nanoparticle to Clinical Medicine. *Br. J. Radiol.* **2019**, *92*, 20180365.

86. Thomas, E.; Colombeau, L.; Gries, M.; Peterlini, T.; Mathieu, C.; Thomas, N.; Boura, C.; Frochot, C.; Vanderesse, R.; Lux, F.; Barberi-Heyob, M.; Tillement, O. Ultrasmall AGuIX theranostic nanoparticles for vascular-targeted interstitial photodynamic therapy of glioblastoma. *Int. J. Nanomed.* **2017**, *12*, 7075–7088.
87. Bridot, J.-L.; Faure, A.-C.; Laurent, S.; Riviere, C.; Billotey, C.; Hiba, B.; Janier, M.; Jossierand, V.; Coll, J.-L.; Elst, L.V.; Muller, R.; Roux, S.; Perriat, P.; Tillement, O. Hybrid Gadolinium Oxide Nanoparticles: Multimodal Contrast Agents for In Vivo Imaging. *J. Am. Chem. Soc.* **2007**, *129*, 5076–5084.
88. Major, J.L.; Meade, T.J. Bioresponsive, Cell-Penetrating, and Multimeric MR Contrast Agents. *Acc. Chem. Res.* **2009**, *42*, 893–903.
89. Longmire, M.; Choyke, P.L.; Kobayashi, H. Clearance Properties of Nano-Sized Particles and Molecules as Imaging Agents. *Nanomedicine* **2008**, *3*, 703–717.
90. Alexis, F.; Pridgen, E.; Molnar, L.K.; Farokhzad, O.C. Factors Affecting the Clearance and Biodistribution of Polymeric Nanoparticles. *Mol. Pharm.* **2008**, *5*, 505–515.
91. Owens, D.E.; Peppas, N.A. Opsonization, Biodistribution, and Pharmacokinetics of Polymeric Nanoparticles. *Int. J. Pharm.* **2006**, *307*, 93–102.
92. Albanese, A.; Tang, P.S.; Chan, W.C.W. The Effect of Nanoparticle Size, Shape, and Surface Chemistry on Biological Systems. *Annu. Rev. Biomed. Eng.* **2012**, *14*, 1–16.
93. Blanco, E.; Shen, H.; Ferrari, M. Principles of Nanoparticle Design for Overcoming Biological Barriers to Drug Delivery. *Nat. Biotechnol.* **2015**, *33*, 941–951.
94. Bertrand, N.; Leroux, J.-C. The Journey of a Drug-Carrier in the Body: An Anatomico-Physiological Perspective. *J. Control. Release* **2012**, *161*, 152–163.
95. Peer, D.; Karp, J.M.; Hong, S.; Farokhzad, O.C.; Margalit, R.; Langer, R. Nanocarriers as an Emerging Platform for Cancer Therapy. *Nat. Nanotechnol.* **2007**, *2*, 751–760.
96. Parang, K.; Nasrolahi Shirazi, A. Peptide-Mediated Cellular Delivery Systems. *Chem. Soc. Rev.* **2013**, *42*, 4120–4133.
97. Roberts, D.R.; Lindhorst, S.M.; Welsh, C.T.; et al. High Levels of Gadolinium Deposition in the Skin of a Patient with Normal Renal Function. *Invest. Radiol.* **2016**, *51*, 280–289.
98. Roberts, D.R.; Holden, K.R. Progressive Increase of T1 Signal Intensity in the Dentate Nucleus and Globus Pallidus on Unenhanced T1-Weighted MR Images in the Pediatric Brain Exposed to Multiple Doses of Gadolinium Contrast. *Brain Dev.* **2016**, *38*(3), 331–336.
99. Choi, H.S.; Liu, W.; Misra, P.; et al. Renal Clearance of Quantum Dots. *Nat. Biotechnol.* **2007**, *25*, 1165–1170.
100. Frenzel, T.; Lengsfeld, P.; Schirmer, H.; Hütter, J.; Weinmann, H.-J. Stability of Gadolinium-Based Magnetic Resonance Imaging Contrast Agents in Human Serum at 37 °C. *Invest. Radiol.* **2008**, *43*, 817–828.
101. Idée, J.-M.; Port, M.; Robic, C.; Medina, C.; Sabatou, M.; Corot, C. Role of Thermodynamic and Kinetic Stability in Gadolinium Chelate Safety. *Invest. Radiol.* **2009**, *44*, 123–133. 94.
102. Rogosnitzky, M.; Branch, S. Gadolinium-Based Contrast Agent Toxicity: A Review of Known and Proposed Mechanisms. *Biomaterials* **2016**, *29*, 365–376.
103. Neburkova, J.; Rulseh, A.M.; Chang, S.L.Y.; Raabova, H.; Vejpravova, J.; Dracinsky, M.; Tarabek, J.; Kotek, J.; Pingle, M.; Majer, P.; Vymazal, J.; Cigler, P. Formation of Gadolinium–Ferritin from Clinical Magnetic Resonance Contrast Agents. *Nanoscale Adv.* **2020**, *2*, 5567–5571.
104. McDonald, R.J.; McDonald, J.S.; Kallmes, D.F.; et al. Gadolinium Deposition in Human Brain Tissues after Contrast-Enhanced MR Imaging in Adult Patients without Intracranial Abnormalities. *Radiology* **2017**, *285*(2), 546–554.
105. Ayers-Ringler, J.; McDonald, J.S.; Connors, M.A.; et al. Neurologic Effects of Gadolinium Retention in the Brain after Gadolinium-Based Contrast Agent Administration. *Radiology* **2022**, *302*(3), 676–683.
106. Tibussek, D.; Rademacher, C.; Caspers, J.; et al. Gadolinium Brain Deposition after Macrocytic Gadolinium Administration: A Pediatric Case-Control Study. *Radiology* **2017**, *285*(1), 223–230.
107. Stojanov, D.A.; Aracki-Trenkic, A.; Vojinovic, S.; Benedeto-Stojanov, D.; Ljubisavljevic, S. Increasing Signal Intensity within the Dentate Nucleus and Globus Pallidus on Unenhanced T1W Magnetic Resonance Images in Patients with Relapsing-Remitting Multiple Sclerosis: Correlation with Cumulative Dose of Gadobutrol. *Eur. Radiol.* **2016**, *26*(3), 807–815.

108. Bjørnerud, A.; Vatnehol, S.A.S.; Larsson, C.; Due-Tønnessen, P.; Hol, P.K.; Groote, I.R. Signal Enhancement of the Dentate Nucleus at Unenhanced MR Imaging after Very High Cumulative Doses of Gadobutrol: An Observational Study. *Radiology* **2017**, *285*(2), 434–444.
109. Radbruch, A.; Weberling, L.D.; Kieslich, P.J.; et al. High-Signal Intensity in the Dentate Nucleus and Globus Pallidus on Unenhanced T1-Weighted Images: Evaluation of Gadobutrol. *Invest. Radiol.* **2015**, *50*(12), 805–810.
110. Murata, N.; Gonzalez-Cuyar, L.F.; Murata, K.; et al. Macrocyclic and Other Non-Group 1 Gadolinium Contrast Agents Deposit Low Levels of Gadolinium in Brain and Bone Tissue: Preliminary Results. *Invest. Radiol.* **2016**, *51*(7), 447–453.
111. Kobayashi, M.; Levendovszky, S.R.; Hippe, D.S.; et al. Comparison of Human Tissue Gadolinium Retention and Elimination between Gadoteridol and Gadobenate. *Radiology* **2021**, *300*(3), 559–569.
112. Le Fur, M.; McDonald, R.J.; Murray, D.L.; Thielen, K.R.; Eckel, L.J.; Jentoft, M.E.; Kallmes, D.F.; Widrick, J.J.; Toland, J.A.; Wagner, B.; et al. Gadolinium-based Contrast Agent Biodistribution and Speciation in Rats and Humans: Comparison of Gadoterate, Gadoteridol, Gadobutrol, and Gadobenate Using MRI, Mass Spectrometry, Elemental Imaging, and Electron Paramagnetic Resonance Spectroscopy. *Radiology* **2023**, *309*, e230984.
113. Guenther, C.; Frenzel, T.; Rottmann, A.; Lohrke, J.; Janssen, W. Pharmacokinetics, Excretion, and Organ Distribution of the Novel Gadolinium-Based MRI Contrast Agent Gadoquatrane in Female Cynomolgus Monkeys. *Invest. Radiol.* **2025**, *60*, 831–839.
114. Kubik-Huch, R.A.; Gottstein-Aalame, N.M.; Frenzel, T.; Seifert, B.; Puchert, E.; Wittek, S.; Debatin, J.F. Gadopentetate Dimeglumine Excretion into Human Breast Milk during Lactation. *Radiology* **2000**, *216*(2), 555–558.
115. Hahn, G.; Sorge, I.; Gruhn, B.; et al. Pharmacokinetics and Safety of Gadobutrol-Enhanced Magnetic Resonance Imaging in Pediatric Patients. *Invest. Radiol.* **2009**, *44*(12), 776–783.
116. Lux, F.; Roux, S.; Perriat, P.; Tillement, O. Gadolinium-Based Nanoparticles for Theranostic MRI-Radiosensitization. *Nanomedicine* **2019**, *14*, 2479–2493.
117. McMahon, S.J.; Hyland, W.B.; Muir, M.F.; Coulter, J.A.; Jain, S.; Butterworth, K.T.; Schettino, G.; Dickson, G.R.; Hounsell, A.R.; O’Sullivan, J.M.; Prise, K.M.; Hirst, D.G.; Currell, F.J. Biological Consequences of Nanoscale Energy Deposition near Irradiated Heavy Atom Nanoparticles. *Sci. Rep.* **2016**, *6*, 33290.
118. Lux, F.; Tran, V.-L.; Thomas, E.; Dufort, S.; Rossetti, F.; Martini, M.; Truillet, C.; Chouikrat, R.; Boschetti, F.; Denat, F.; Roux, S.; Perriat, P.; Tillement, O. AGuIX® Gadolinium-Based Nanoprobes for Theranostic Applications. *Theranostics* **2014**, *4*, 625–635.
119. Le Duc, G.; Miladi, I.; Alric, C.; Mowat, P.; Bräuer-Krisch, E.; Bouchet, A.; Khalil, E.; Bilottey, C.; Janier, M.; Lux, F.; Epicier, T.; Perriat, P.; Roux, S.; Tillement, O. Toward an image-guided microbeam radiation therapy using gadolinium-based nanoparticles. *ACS Nano* **2011**, *5*, 9566–9574.
120. Aubrun, C.; Doussineau, T.; Carmès, L.; Meyzaud, A.; Boux, F.; Dufort, S.; Delfour, A.; De Beaumont, O.; Mirjolet, C.; Le Duc, G. Mechanisms of Action of AGuIX as a Pan-Cancer Nano-Radiosensitizer: A Comprehensive Review. *Pharmaceuticals* **2025**, *18*, 519.
121. Chen, H.; Zhang, L.; Li, Y.; Wang, J. Nanomaterials for photothermal therapy: An update. *Nanoscale* **2016**, *8*, 5567–5583.
122. Jaque, D.; Martínez Maestro, L.; del Rosal, B.; Haro-González, P.; Benayas, A.; Plaza, J. L.; Rodríguez, E. M.; García Solé, J. Nanoparticles for photothermal therapies. *Nanoscale* **2014**, *6*, 9494–9530.
123. Lv, X.; Wang, X.; Li, T.; Wei, C.; Tang, Y.; Yang, T.; Wang, Q.; Yang, X.; Chen, H.; Shen, J.; Yang, H.; Ke, H. Rationally designed monodisperse Gd<sub>2</sub>O<sub>3</sub>/Bi<sub>2</sub>S<sub>3</sub> hybrid nanodots for efficient cancer theranostics. *Small* **2018**, *14*, 1802904.
124. Jain, A.; Fournier, P. G. J.; Mendoza-Lavaniegos, P.; Sengar, P.; Guerra-Olvera, F. M.; Iñiguez, E.; Kretzschmar, T. G.; Hirata, G. A.; Juárez, P. Functionalized Gd<sub>2</sub>O<sub>3</sub> nanoparticles for magnetic resonance imaging and targeted photothermal therapy of cancer. *J. Nanobiotechnol.* **2018**, *16*, 26.
125. Hildebrandt, B.; Wust, P.; Ahlers, O.; Dieing, A.; Sreenivasa, G.; Kerner, T.; Felix, R.; Riess, H. The cellular and molecular basis of hyperthermia. *Crit. Rev. Oncol. Hematol.* **2002**, *43*, 33–56.

126. Huang, X.; Jain, P. K.; El-Sayed, I. H.; El-Sayed, M. A. Plasmonic photothermal therapy (PPTT) using gold nanoparticles. *Lasers Med. Sci.* **2008**, *23*, 217–228.
127. Fan, W.; Yung, B.; Huang, P.; Chen, X. Nanotechnology for multimodal synergistic cancer therapy. *Chem. Rev.* **2017**, *117*, 13566–13638.
128. Liu, Y.; Bhattarai, P.; Dai, Z.; Chen, X. Photothermal therapy and immunotherapy: A synergistic combination. *ACS Nano* **2018**, *12*, 2493–2505.
129. Zhao, P.-P.; Ge, Y.-W.; Liu, X.-L.; Ke, Q.-F.; Zhang, J.-W.; Zhu, Z.-A.; Guo, Y.-P. Ordered Arrangement of Hydrated GdPO<sub>4</sub> Nanorods in Magnetic Chitosan Matrix Promotes Tumor Photothermal Therapy and Bone Regeneration against Breast Cancer Bone Metastases. *Chem. Eng. J.* **2020**, *381*, 122694.
130. Cui, H.; Zhao, Y.-Y.; Wu, Q.; You, Y.; Lan, Z.; Zou, K.-L.; Cheng, G.-W.; Chen, H.; Han, Y.-H.; Chen, Y.; Qi, X.-D.; Meng, X.-W.; Ma, L.-M.; Yu, G.-T. Microwave-Responsive Gadolinium Metal–Organic Framework Nanosystem for MRI-Guided Cancer Thermotherapy and Synergistic Immunotherapy. *Bioact. Mater.* **2024**, *33*, 532–544.
131. Jiang, Q.; Liu, L.; Li, Q.; Cao, Y.; Chen, D.; Du, Q.; Yang, X.; Huang, D.; Pei, R.; Chen, X.; Huang, G. NIR-Laser-Triggered Gadolinium-Doped Carbon Dots for Magnetic Resonance Imaging, Drug Delivery and Combined Photothermal Chemotherapy for Triple-Negative Breast Cancer. *J. Nanobiotechnol.* **2021**, *19*, 64.
132. Bertrand, N.; Wu, J.; Xu, X.; Kamaly, N.; Farokhzad, O.C. Cancer Nanotechnology: The Impact of Passive and Active Targeting in the Era of Modern Cancer Biology. *Adv. Drug Deliv. Rev.* **2014**, *66*, 2–25.
133. Mowat, P.; Mignot, A.; Rima, W.; Lux, F.; Tillement, O.; Roulin, C.; Dutreix, M.; Bechet, D.; Huger, S.; Humbert, L.; Barberi-Heyob, M.; Aloy, M.-T.; Armandy, E.; Rodriguez-Lafresse, C.; Le Duc, G.; Roux, S.; Perriat, P. In Vitro Radiosensitizing Effects of Ultrasmall Gadolinium-Based Particles on Tumour Cells. *J. Nanosci. Nanotechnol.* **2011**, *11*, 7833–7839.
134. Detappe, A.; Thomas, E.; Tibbitt, M.W.; Kunjachan, S.; Zavidij, O.; Parnandi, N.; Reznichenko, E.; Lux, F.; Tillement, O.; Berbeco, R. Ultrasmall Silica-Based Bismuth Gadolinium Nanoparticles for Dual Magnetic Resonance–Computed Tomography Image-Guided Radiation Therapy. *Nano Lett.* **2017**, *17*, 1733–1740.
135. Siribbal, S.M.; Jurewicz, A.; Hassan, M.; Iqbal, S.; Hu, Z.; Uvdal, K.; Hussain, M.S.; Mathur, S.; Ilyas, S. Biocompatible Hollow Gadolinium Oxide Nanocarriers for the Transport of Bioactive Molecules to Cells. *ACS Appl. Nano Mater.* **2024**, *7*, 12408–12419.
136. Kumar, A.; Sarkar, T.; Solanki, P.R. Amine Functionalized Gadolinium Oxide Nanoparticles-Based Electrochemical Immunosensor for Cholera. *Biosensors* **2023**, *13*, 177.
137. Siribbal, S.M.; Ilyas, S.; Renner, A.M.; Iqbal, S.; Muñoz Vázquez, S.; Moawia, A.; Valldor, M.; Hussain, M.S.; Schomäcker, K.; Mathur, S. Click Functionalized Biocompatible Gadolinium Oxide Core–Shell Nanocarriers for Imaging of Breast Cancer Cells. *RSC Adv.* **2022**, *12*, 31830–31845.
138. Mi, P. Stimuli-Responsive Nanocarriers for Drug Delivery, Tumor Imaging, Therapy and Theranostics. *Theranostics* **2020**, *10*, 4557–4588.
139. Ganesh, S.K.; Chakravorty, A.; Raghavan, V.; Subathra Devi, C. Chitosan-Coated ZnO/TiO<sub>2</sub>/Gd<sub>2</sub>O<sub>3</sub> Nanocomposites for Improved Rapamycin Delivery in Non-Small Cell Lung Cancer. *Int. J. Biol. Macromol.* **2025**, *319*, 145439.
140. Babayevska, N.; Kustrzyńska, K.; Przysiecka, Ł.; Jarek, M.; Jancelewicz, M.; Iatsunskyi, I.; Dydak, K.; Skupin-Mrugalska, P.; Janiszewska, E. Doxorubicin and ZnO-Loaded Gadolinium Oxide Hollow Spheres for Targeted Cancer Therapy and Bioimaging. *Spectrochim. Acta A Mol. Biomol. Spectrosc.* **2025**, *333*, 125903.
141. Wei, Z.; Wu, M.; Li, Z.; Lin, Z.; Zeng, J.; Sun, H.; Liu, X.; Liu, J.; Li, B.; Zeng, Y. Gadolinium-Doped Hollow CeO<sub>2</sub>–ZrO<sub>2</sub> Nanoplatform as Multifunctional MRI/CT Dual-Modal Imaging Agent and Drug Delivery Vehicle. *Drug Deliv.* **2018**, *25*, 353–363.
142. Sun, X.; Kou, B. Biocompatibility and Potential Anticancer Activity of Gadolinium Oxide (Gd<sub>2</sub>O<sub>3</sub>) Nanoparticles against Nasal Squamous Cell Carcinoma. *BMC Biotechnol.* **2024**, *24*, 53.
143. Butterworth, K.T.; McMahon, S.J.; Currell, F.J.; Prise, K.M. Physical Basis and Biological Mechanisms of Gold Nanoparticle Radiosensitization. *Nanotechnology* **2012**, *23*, 295101.
144. Rétif, P.; Pinel, S.; Toussaint, M.; Frochot, C.; Chouikrat, R.; Bastogne, T.; Barberi-Heyob, M. Nanoparticles for Radiation Therapy Enhancement: The Key Parameters. *Cancer Nanotechnol.* **2015**, *6*, 1–16.

145. Her, S.; Jaffray, D.A.; Allen, C. Gold Nanoparticles for Applications in Cancer Radiotherapy: Mechanisms and Recent Advancements. *Theranostics* **2017**, *7*, 225–239.
146. Jackson, S.P.; Bartek, J. The DNA-Damage Response in Human Biology and Disease. *Nature* **2009**, *461*, 1071–1078.
147. Wang, Y.; Yang, T.; Ke, H.; Zhu, A.; Wang, Y.; Wang, J.; Shen, J.; Liu, G.; Chen, C.; Zhao, Y. Smart Albumin-Biomaterialized Nanocomposites for Multimodal Imaging and Photothermal Tumor Ablation. *Biomaterials* **2018**, *160*, 57–68.
148. Pawlik, T.M.; Keyomarsi, K. Role of Cell Cycle in Chemotherapy Sensitivity. *J. Clin. Oncol.* **2004**, *22*, 4436–4445.
149. American College of Radiology. *ACR Manual on Contrast Media*; Version 2024; American College of Radiology: Reston, VA, USA, **2024**.

**Disclaimer/Publisher's Note:** The statements, opinions and data contained in all publications are solely those of the individual author(s) and contributor(s) and not of MDPI and/or the editor(s). MDPI and/or the editor(s) disclaim responsibility for any injury to people or property resulting from any ideas, methods, instructions or products referred to in the content.